Short-term and Inter-annual Variations of Migrating Diurnal and Semidiurnal Tides in the Mesosphere and Lower Thermosphere

Manbharat S. Dhadly[1], John T. Emmert[2], Douglas P. Drob[2], John P. McCormack[2], and Rick J. Niciejewski[3]

[1]National Research Council Postdoctoral Research Associate, Space Science Division, Naval Research Laboratory, Washington DC, USA
[2]Space Science Division, Naval Research Laboratory, Washington DC, USA
[3]Climate and Space Sciences and Engineering, University of Michigan, Ann Arbor, Michigan, USA

Key Points:

- Short-term and intra-annual variability in DW1 and SW2 tidal modes estimated from TIDI and NAVGEM-HA are in good agreement.
- The biennial oscillations in DW1 and SW2 modes are systematically correlated with equatorial stratospheric quasi-biennial oscillation.
- There is no clear evidence of any solar cycle dependence or long-term trend in either DW1 or SW2 modes.

This is the author manuscript accepted for publication and has undergone full peer review but has not been through the copyediting, typesetting, pagination and proofreading process, which may lead to differences between this version and the Version of Record. Please cite this article as doi: 10.1029/2018JA025748

Corresponding author: Manbharat Dhadly, manbharat.dhadly.ctr@nrl.navy.mil

Abstract

Among the broad spectrum of vertically propagating tides, migrating diurnal (DW1) and semidiurnal (SW2) are prominent modes of energetic and dynamical coupling between the MLT and the upper thermosphere and ionosphere. DW1 and SW2 tides are modulated on time scales ranging from days to years. NASA TIMED is the first observational platform to perform global synoptic observations of these fundamental tides (for nearly two decades) overcoming previous observational limitations. . Here, we utilize the extensive archive of TIDI wind measurements and exploit the capabilities of tidal theory to estimate short-term (<1 month), seasonal (intra-annual), long-term (>1 year), and climatological variability in DW1 (1,1), SW2 (2,2), and SW2 (2,3) modes and then compare with tidal estimates derived from the Navy Global Environmental Model - High Altitude version (NAVGEM-HA) data assimilation system. Overall, the tidal estimates from TIDI and NAVGEM-HA are similar and exhibit significant short-term and intra-annual variability. The short-term variability can induce ~64% change in the DW1 amplitude. Statistically, the short-term variability in DW1 (1,1), SW2 (2,2), and SW2 (2,3) modes is of the order of ~9 m/s, 33 m/s, and 20 m/s, respectively. The biennial oscillations in DW1 and SW2 modes suggests a systematic correlation with the equatorial quasi-biennial oscillation (QBO) in the stratosphere, and are more apparent in DW1 amplitudes. Although there is significant interannual variability in addition to the apparent biennial signal, there is no clear evidence of any solar cycle dependence or long-term trend in either DW1 or SW2 modes.

1 Introduction

Atmospheric solar tides are oscillations of temperature, winds, and composition with periods that are harmonics of 1 day. The migrating tides (sun synchronous) are excited by absorption of: solar infrared (IR) radiation by water vapor in the troposphere, ultraviolet (UV) radiations by ozone in the stratosphere, and UV and extreme-ultraviolet (EUV) radiation in the thermosphere [e.g., *Forbes*, 1982a,b] . As the tidal oscillations propagate vertically, away from their source regions in troposphere and stratosphere, other processes such as latent heat release due to deep convection in the tropics, nonlinear interaction between global-scale waves, interaction between tides and gravity waves, and nonlinear interactions associated with the background zonal mean winds modulate the radiatively excited atmospheric tides on various temporal and spatial scales [e.g., *Forbes and Garrett*, 1979; *Oberheide et al.*, 2002; *Hagan and Forbes*, 2003; *Yigit and Medvedev*, 2015]. This variability of the lower atmosphere is imprinted on upwardly propagating tidal components and modulates properties of the thermosphere and the ionosphere [e.g., *Lieberman et al.*, 1994; *Oberheide and Forbes*, 2008; *Forbes*, 2009; *Hagan et al.*, 2009; *Häusler and Luhr*, 2009; *Oberheide et al.*, 2015]. Tides are also perceived as important coupling agents between the MLT (mesosphere and lower thermosphere) region and ionosphere [e.g., *England et al.*, 2006; *Immel et al.*, 2006; *Jin et al.*, 2012; *Pedatella et al.*, 2012]. They can modulate gravity wave momentum and energy deposition by filtering small-scale gravity waves, interact with planetary waves, induce variability in polar mesospheric clouds, modulate equatorial vertical plasma drifts and bubble seeding, and contribute to neutral density variability [e.g., *Fritts et al.*, 1987; *Beard et al.*, 1999; *Fiedler et al.*, 2005; *Oberheide et al.*, 2009, 2011; *Beldon and Mitchell*, 2010; *Chang et al.*, 2011; *Fang et al.*, 2013].

The past three decades of research has corroborated the importance of atmospheric tides in dynamical coupling between the lower and upper atmosphere. Studies have shown that there is a considerable amount of unexplained day-to-day variability in the thermosphere and ionosphere (TI) [e.g., *Mendillo et al.*, 2002] that often competes with the variability caused by other factors such as geomagnetic activity and solar flux changes. Meteorological variations in the lower atmosphere propagate into the TI system, accounting for an estimated 10–50% of day-to-day TI variability [*Forbes et al.*, 2000; *Mendillo*

et al., 2002; *Fang et al.*, 2013; *Liu et al.*, 2016] and interrupts communication and navigation systems.

Among the spectrum of upward propagating waves, the vertically propagating migrating diurnal and semidiurnal tides are particularly influential. They are considered the primary source of quiet-time low-latitude electric fields in the ionosphere [*Millward et al.*, 2001; *Yamazaki et al.*, 2016], and they modulate thermospheric composition [*Yamazaki and Richmond*, 2013; *Yamazaki et al.*, 2016]. Model simulations by *Fang et al.* [2013] indicate that day-to-day variations of semidiurnal tides in the MLT are associated with ~30% variations in peak equatorial vertical plasma drifts. Changes in diurnal and semidiurnal tides in the MLT have also been implicated in the TI response to stratospheric sudden warmings (SSWs) [*Pedatella et al.*, 2016], but their amplitudes and phases exhibit large variability even in the absence of SSWs. Currently, there is little observational knowledge of the coupling on short time scales (<1 month) because spectral analysis of the existing satellite data typically requires a month or longer to sample the full range of local times [e.g., *Oberheide et al.*, 2011]. Ground-based measurements cannot resolve non-migrating tidal variations from the migrating tidal variations without measurements from multiple longitudinally distributed stations at similar latitudes [e.g., *Oberheide et al.*, 2006; *Ward et al.*, 2010].

Atmospheric tides show both long-term and short-term variability. Observational studies combined with advances and increasing reliability of GCMs have exposed their fundamental sources, their inter-annual, latitudinal, and altitudinal characteristics, and their association with variability in the Earth's ionosphere and thermosphere. Despite their perceived impact on the TI dynamics, their short-term variability (on the time scales smaller than a month) and role in coupling the lower atmosphere with ionosphere and thermosphere is still largely unknown. The migrating diurnal and semidiurnal tides propagating vertically can be impacted by a number of sources which can modify their amplitude and phase. In particular, the major focus of this study is to investigate short-term (<1 month) variability in the migrating diurnal (DW1) and semidiurnal (SW2) tides that have received little attention in the literature. In addition, we discuss their seasonal or intra-annual (<1 year), long-term (>1 year), and climatological variability, using space-based wind measurements and a physics-based data assimilation model.

A number of space-based observational MLT tidal studies have used NASA Thermosphere-Ionosphere-Mesosphere Energetic and Dynamics/Sounding of the Atmosphere using Broadband Emission Radiometry (TIMED/SABER) temperatures [e.g., *Huang et al.*, 2006; *Wu et al.*, 2008; *Mukhtarov et al.*, 2009; *Nguyen and Palo*, 2013; *Riggin and Lieberman*, 2013; *Truskowski et al.*, 2014]. Others have used Microwave Limb Sounder (MLS) on the EOS Aura spacecraft and High Resolution Doppler Imager (HRDI) on the Upper Atmosphere Research Satellite (UARS) [e.g., *Hays et al.*, 1994; *Burrage et al.*, 1995; *Forbes et al.*, 2006; *Nguyen and Palo*, 2013]. Many ground-based short-term and long-term variability studies of MLT diurnal and semidiurnal tides have used radar winds [e.g., *Chang and Avery*, 1997; *Vincent et al.*, 1998; *Jacobi et al.*, 1999; *Buriti et al.*, 2008; *Kumar et al.*, 2008; *Gurubaran et al.*, 2009; *Sridharan et al.*, 2010; *Davis et al.*, 2013]. *Friedman et al.* [2009] and *Yuan et al.* [2008] studied solar semidiurnal tidal perturbation using LIDARs. *Hernandez et al.* [1993] and *Niciejewski and Killeen* [1995] studied semidiurnal tides using ground-based Fabry-Perot Interferometers (FPI). Many other studies have estimated long-term and climatological trends in tides from TIMED Doppler Interferometer (TIDI) winds [e.g., *Oberheide et al.*, 2006, 2009, 2011; *Wu et al.*, 2008]. Nevertheless, only few studies [e.g., *Niciejewski et al.*, 2006] have explored TIDI winds for estimating short-term day-to-day variability in MLT tides. This is primarily due to the limited local time sampling over short time periods and gaps in the data associated with solar beta angle selection criteria (discussed later). Due to the precession rate of the TIMED orbit, TIDI samples all local times in 60 days. Consequently, most of the TIDI wind based tidal estimation studies [e.g., *Forbes et al.*, 2008; *Wu et al.*, 2008; *Mukhtarov et al.*, 2009; *Truskowski et al.*, 2014]

are focused on either a 30 day or 60 day running average window or seasonal and long-term variations.

Ground-based platforms provide continuous tidal information but no spatial information. The ground-based observations have described day-to-day variability in tidal oscillations quite extensively, but it is impossible to de-alias non-migrating and migrating tides from the observations without measurements from multiple longitudinally distributed stations at similar latitudes [*Ward et al.*, 2010]. On the other hand, space-based observations provide limited spatiotemporal coverage that is usually considered insufficient to directly extract short-term tidal variability. The primary focus of this study is to take advantage of the knowledge gained from earlier tidal studies and utilize the TIDI MLT wind measurements by exploiting the physical constraint of Hough functions to estimate the short-term variability in migrating diurnal DW1 (westward, wave number 1 – (1,1) mode) and migrating semidiurnal SW2 (westward, wave number 2 – (2,2) and (2,3) modes) tides. Hough modes are eigen solutions of Laplace's tidal equation and define the horizontal structure of each vertically propagating class of tidal modes. These modes are excited in the lower atmosphere and propagate upward; the physics and underlying mathematical theory of these mode excitations, propagation, altitudinal dominance, and dissipation are presented in *Forbes* [1982a,b].

Despite the sparse local time coverage of TIDI over time periods less than a month, it is possible to obtain short-term tidal estimates [e.g., *Hays et al.*, 1994; *Burrage et al.*, 1995; *Niciejewski et al.*, 2006; *Ortland*, 2017]. This is because the latitudinal profiles of diurnal and semidiurnal MLT tidal modes are well represented using orthogonal Hough functions. This study includes TIDI winds from 2002 to 2016, allowing us to investigate DW1 and SW2 variability over a wide range of time scales.

Further, we compare TIDI-derived estimates of tidal variability over interseasonal time scales for 2010 with similar estimates based on assimilated wind fields from the Navy Global Environmental Model - High Altitude version (NAVGEM-HA). Our comparison of TIDI tidal estimates during 2010 with NAVGEM-HA serves as an independent validation of the estimation process as NAVGEM-HA does not directly assimilate any MLT wind data. We also include tidal estimates from the Horizontal Wind Model (HWM14). HWM14 is a climatological model and did not include any wind data from TIDI. Thus, all three wind data sets in this comparison are independent.

Multiple studies [e.g., *Burrage et al.*, 1995; *Lieberman*, 1997; *Hagan et al.*, 1999; *Huang et al.*, 2006; *Wu et al.*, 2008; *Xu et al.*, 2009; *Gurubaran et al.*, 2009; *Mukhtarov et al.*, 2009; *Davis et al.*, 2013; *Nguyen and Palo*, 2013; *Laskar et al.*, 2016] have reported interannual oscillations of the diurnal and semidiurnal tides that closely resemble the stratospheric quasi-biennial oscillation (QBO), suggesting modulation of upward propagating tides by QBO. The QBO is the characteristic mean flow behavior of zonal winds in the tropical stratosphere-mesosphere system. Studies have shown that QBO interaction with tides could dampen or enhance the tides [e.g., *Andrews et al.*, 1987; *Hamilton and Hamilton*, 1998; *Mayr and Mengel*, 2005]. The long time stretch of this study provides an unprecedented opportunity to explore any systematic long-term teleconnections between stratospheric QBO and MLT tides (DW1 and SW2 modes).

Solar activity dramatically affects geospace weather and plays an important role in determining the state of Earth's atmosphere. Thus, solar activity is expected to have some influence on many atmospheric phenomena such as tides [e.g., *Sridharan et al.*, 2010; *Laskar et al.*, 2016; *Singh and Gurubaran*, 2017]. However, many existing studies of MLT migrating tides [e.g., *Fraser et al.*, 1989; *Bremer et al.*, 1997, and thereafter] indicate no statistically significant correlation between tide amplitude and solar activity. In this study, which covers the more than a solar cycle, we revisit long-term variations in MLT tides associated with the solar cycle.

The paper is organized as follows. Section 2 discusses TIDI and NAVGEM-HA data, section 3 describes the methodology used for tidal extraction from TIDI, NAVGEM-HA, and HWM14. The extracted short-term, seasonal, long-term, and climatological variability and trends in the DW1 and SW2 tidal components are described in detail in section 4. Finally, section 5 summarizes and discusses the results.

2 Data

The MLT region horizontal neutral winds measured by TIMED/TIDI from 2002 to 2016 are used, in combination with the NAVGEM-HA and HWM14 horizontal neutral winds for 2010. The TIDI instrument is a limb-scanning Fabry-Perot interferometer designed to study the MLT region daytime and nighttime horizontal neutral wind dynamics on a global basis (pole-to-pole). The TIMED satellite was launched in December 2001 and all four instruments continue to produce valuable scientific measurements at the time of this publication. TIDI uses four individual scanning telescopes for four different look directions each covering an altitude range of ~70–120 km. The field of view of each TIDI telescope is 2.5 deg horizontal by 0.05 deg vertical providing a resolution of ~2 km over the altitude range ~70–120 km. Four orthogonal telescopes, two on either side of the TIMED orbital path, view the limb simultaneously in two narrow swaths separated by ~30 deg longitude at low latitudes. The emissions viewed are individual O_2 Atmospheric (0,0) lines which emit both dayglow and nightglow in the MLT. The TIMED orbit precesses such that TIDI measurements return to the same latitude and local time coordinates after one year, which facilitates de-seasonalization of the data for long-term studies. An overview of TIDI instrumental design, orbital geometry, operational and wind data processing algorithms, and output wind data is presented in *Killeen et al.* [1999, 2006] and *Niciejewski et al.* [2006]. Due to the precession rate, it takes TIDI 60 days to fully sample all local times.

The TIDI measurements suffer from twilight contamination, so we exclude TIDI data when the solar beta angle (the angle between the orbital plane and the Earth-Sun vector) is greater than 55 degrees; i.e., when TIMED orbiting near the terminator. The variation of solar beta angle as a function of day of year 2010 is shown in Figure S1 (given in supporting information). The solar beta angle changes almost at the rate of 3 deg/day except near the turnaround dates. The data elimination associated with high solar beta angles create a gap of roughly 3 weeks during four of the six yaw cycles, centered at the middle of February, April, August, and October each year. Despite the periods of degraded data at high solar beta angles, TIDI winds are the longest continuous wind dataset available from any space-based instrument.

NAVGEM-HA is a numerical weather prediction system designed for middle atmosphere research that combines a hybrid four-dimensional variational (4DVAR) data assimilation (DA) system [*Kuhl et al.*, 2013] with a global semi-implicit semi-Lagrangian forecast model [*Hogan et al.*, 2014]. The DA component of NAVGEM-HA assimilates both standard operational meteorological observations in the troposphere and lower stratosphere plus satellite-based observations of temperature, ozone and water vapor in the stratosphere and mesosphere. NAVGEM-HA does not directly assimilate any middle atmospheric wind measurements; instead, the DA algorithm produces wind increments in balance with the assimilated temperature increments based on a modified form of the gradient wind approximation [*McCormack et al.*, 2014]. The resulting horizontal wind fields are further constrained by the physical parameterizations in the model (e.g., gravity wave drag, diffusion, etc.).

McCormack et al. [2017] recently validated the NAVGEM-HA winds using independent meteor radar wind observations from nine different sites ranging from 69°N–67°S latitude during the boreal winters of 2009–2010 and 2012–2013. The results of this study show that NAVGEM-HA accurately captures the key features of MLT winds during these

periods, particularly the amplitude and phase of the diurnal and semidiurnal tides in upper mesosphere.

NAVGEM-HA outputs data every three hours on a global 1–degree latitude/longitude grid; this sampling frequency in local time is well above the Nyquist sampling frequency for the evaluation of DW1 and SW2 tides. For this study, NAVGEM-HA analyzed wind and geopotential height output on constant pressure levels throughout the MLT region were used to produce zonal and meridional wind fields at fixed geometric altitude levels. Unfortunately, at present, NAVGEM-HA winds are only available over a continuous 12 month period for the year of 2010. Efforts are underway to extend NAVGEM-HA time coverage to other years. As described in *McCormack et al.* [2017] and references therein, a major SSW occurred in early February 2010, which was preceded by a reversal in mesospheric winds at 60°N latitude two weeks earlier beginning on 27 January 2010. The changes in MLT due to the 2010 SSW have been associated with dramatic changes in the composition and dynamics of the thermosphere/ionosphere system [e.g., *Goncharenko et al.*, 2013] through proposed modulation of migrating tides [e.g., *Pedatella et al.*, 2016]. Examining the tidal variability in NAVGEM-HA wind fields during the 2010 period serves as an independent test of the DW1 and SW2 tidal variability estimates over both short-term (days to weeks) and seasonal time scales derived using TIDI winds.

In order to investigate the teleconnection between the stratospheric QBO and MLT tides, we used monthly mean stratospheric zonal winds from 2002 to 2016 at 30hPa obtained from the Singapore radiosonde station (`http://www.geo.fu-berlin.de/en/met/ag/strat/produkte/qbo/index.html`).

3 Methodology

As TIDI takes almost 60 days to fully sample a complete diurnal cycle, most previous tidal variability studies based on TIDI data are either climatological or subject to an assumption that the mean winds during 30-day period are constant. However, ground-based radar studies (mentioned in the introduction section) have shown the presence of significant day-to-day variability in tides. Here, we quantitatively assess the short-term variability in tides by applying the similar Hough mode analysis approach discussed in *Hays et al.* [1994] and *Niciejewski et al.* [2006] to the TIDI winds to derive a 15-year database of tidal variability. The approach for estimating amplitude and phase is based on fitting Hough functions as a representation of tidal latitudinal structure and simple harmonic functions (sine and cosine) as a presentation of their local time variation.

From classical tidal theory, the solution of Laplace's tidal equation may be decomposed into classical Hough modes. Hough functions (eigensolutions of Laplace's tidal equation) define the horizontal structure of each vertically propagating tidal mode with an equivalent depth (eigenvalue of each mode) that defines their vertical structure [*Chapman and Lindzen*, 1970; *Lindzen and Chapman*, 1979]. The vertical wavelength of each mode is estimated from the equivalent depth [e.g., *Forbes*, 1995]. Theoretical and experimental studies of tides [e.g., *Forbes et al.*, 1976; *Lindzen et al.*, 1977; *Forbes and Hagan*, 1982; *Forbes and Groves*, 1987; *Hays et al.*, 1994; *Ortland*, 2005; *Truskowski et al.*, 2014] have shown that the latitudinal structures of diurnal and semidiurnal amplitudes in the MLT region are well characterized in terms of Hough modes. Hough modes change shape (mostly above 100 km) with the change in tidal dissipation (e.g., associated with ion drag, molecular and eddy viscosity and conductivity, and radiative damping) or when mean wind flow is present above the region of wave forcing [*Forbes and Hagan*, 1982]. Thus, the propagation of tides from the lower atmosphere into the thermosphere is commonly explored using Hough Mode Extensions (HMEs) [*Lindzen et al.*, 1977; *Forbes*, 1982a,b; *Forbes and Hagan*, 1982]; HMEs deal with changes in the Hough mode shapes as they encounter dissipation in the thermosphere. *Hays et al.* [1994] showed that the meridional diurnal (1,1) Hough mode retains its shape well in the MLT region below 100 km. Strong zonal mean

zonal wind flows prevail in the MLT region and Hough modes are prone to contamination from mean flows, therefore, we have limited our tidal extraction scheme (as discussed in detail in *Hays et al.* [1994]) to only meridional winds. Previous studies [e.g., *Davis et al.*, 2013] also have shown that migrating tidal signatures estimated from meridional winds are stronger than zonal winds and match better with ground-based measurements [e.g., *Singh and Gurubaran*, 2017].

In the MLT region, the DW1 dominates at tropical latitudes, whereas SW2 peaks at middle latitudes [e.g., *Forbes*, 1995]. Also, a gradual blending of diurnal and semidiurnal tides occurs at high latitudes. For this study, tidal extractions were performed twice, once for DW1 (by fitting DW1 and SW2 modes together and limiting the fitting analysis to latitudes between ±35°) and once for SW2 (2,2) and (2,3) modes (by fitting DW1 and SW2 together and limiting the fitting analysis to latitudes between 25°N and 60°N). Therefore, to avoid any cross-contamination between the migrating diurnal and semidiurnal tides, our analysis of DW1 is limited to latitudes between ±35° latitude, and our SW2((2,2) and (2,3) modes) analysis covers latitudes between 25°N and 60°N (SW2 modes for 25°S to 60°S are shown in Figure S2). In addition, the selected latitudinal ranges avoid aliasing from stationary planetary waves poleward of ±65° [*Oberheide et al.*, 2011]. The peak amplitude of the upward propagating DW1 occurs between 80 km and 100 km, whereas SW2 peaks at slightly higher altitudes [e.g., *Wu et al.*, 2011; *Shepherd et al.*, 2012]. Here, we have estimated DW1 and SW2 modes using TIDI and NAVGEM-HA wind data from 80 km and 95 km for DW1 and 85 km to 100 km for SW2. For a climatological perspective, HWM14 winds were evaluated at 90 km for DW1 and SW2 modes. For tidal extraction, we apply similar data sorting and analysis schemes (described below) to TIDI, NAVGEM-HA, and HWM14 meridional winds. Here, we have not included amplitude growth with altitude (a factor used in *Hays et al.* [1994] and *Niciejewski et al.* [2006]) in the tidal analysis; thus the tidal components extracted in this study represent the average tidal amplitudes in the selected altitude ranges.

For daily extraction of DW1 and SW2 amplitude and phase information from the TIDI, NAVGEM-HA, and HWM14 meridional winds, we employed the dominant diurnal (1,1) and semidiurnal (2,2) and (2,3) Hough mode meridional expansion functions to represent their latitudinal structure [e.g., *Forbes*, 1982a,b]. The latitudinal structures of DW1 and SW2 Hough meridional expansion functions used here, calculated using *Wang et al.* [2016], are shown in Figure 1. Their distinct latitudinal structures allow resolution of the diurnal and semidiurnal tidal behaviors. DW1 and SW2 modes are fitted simultaneously in order to avoid aliasing. We fitted TIDI, NAVGEM-HA, and HWM14 meridional winds to the following function:

$$V = A_0 + H_{(1,1)}(\theta)\left[A_1\cos(\frac{2\pi t}{24}+\frac{2\pi z}{\lambda_{z1}}) + A_2\sin(\frac{2\pi t}{24}+\frac{2\pi z}{\lambda_{z1}})\right] + H_{(2,2)}(\theta)\left[A_3\cos(\frac{2\pi t}{12}+\frac{2\pi z}{\lambda_{z2}}) + A_4\sin(\frac{2\pi t}{12}+\frac{2\pi z}{\lambda_{z2}})\right] + H_{(2,3)}(\theta)\left[A_5\cos(\frac{2\pi t}{12}+\frac{2\pi z}{\lambda_{z3}}) + A_6\sin(\frac{2\pi t}{12}+\frac{2\pi z}{\lambda_{z3}})\right]$$

where $H_{(1,1)}$, $H_{(2,2)}$, and $H_{(2,3)}$ are the diurnal (1,1), semidiurnal (2,2), and semidiurnal (2,3) Hough meridional expansion functions respectively; λ_{z1}, λ_{z2}, and λ_{z3} are the vertical wavelengths for diurnal (1,1), semidiurnal (2,2), and semidiurnal (2,3) modes respectively; $(A_0, A_1, A_2, A_3, A_4, A_5, A_6)$ are the coefficients; θ is latitude, t is local solar time, and z is the altitude. The coefficients are estimated by least square fitting and are used for calculating amplitudes of the diurnal (1,1) and semidiurnal (2,2) and (2,3) modes given by $\sqrt{A_1^2+A_2^2}$, $\sqrt{A_3^2+A_4^2}$, and $\sqrt{A_5^2+A_6^2}$ respectively. Similarly, the phases of diurnal (1,1) and semidiurnal (2,2) and (2,3) modes are calculated using $\frac{24}{2\pi}\tan^{-1}(\frac{A_2}{A_1})$, $\frac{12}{2\pi}\tan^{-1}(\frac{A_4}{A_3})$, and $\frac{12}{2\pi}\tan^{-1}(\frac{A_6}{A_5})$ respectively. The mean vertical wavelength for the diurnal (1,1) mode is 23 km (as in *Hays et al.* [1994] and *Burrage et al.* [1995]). For the semidiurnal (2,2) and (2,3) modes, vertical wavelengths of 311 km and 81.4 km, respectively, from the classical tidal theory [as in *Forbes and Groves*, 1987; *Yuan et al.*, 2008; *Truskowski et al.*, 2014]

were used. It is important to note that the amplitudes calculated here are the peak amplitude of tidal modes with respect to latitude and the phases are the local time of maximum amplitudes, as discussed in *Hays et al.* [1994], *Burrage et al.* [1995], and *Niciejewski et al.* [2006]. The extracted tidal fields are included in the supporting information. These tidal fitting analyses are carried out in time and latitude by fitting data from all the altitudes selected for DW1 and SW2 modes; thus we expect our space-time decomposition to be mostly alias-free. However, we do not exclude any possibility of aliasing in TIDI fits from planetary waves. But fitting data with Hough modes and a good agreement with fully sampled data from NAVGEM-HA (discussed later) reduces the possibility of aliasing in the TIDI results. As a verification test of our analysis, we reproduced the DW1 tidal amplitudes using TIDI meridional winds shown in Figure 12b of *Killeen et al.* [2006] and Figure 19 of *Niciejewski et al.* [2006].

To investigate the inter-annual, long-term, and climatological variation of tides (e.g., QBO and solar cycle related variations), we averaged the annual tidal amplitudes as a function of day of year from 2002 to 2016 and calculated a composite daily mean amplitude profile. The composite daily mean profile embodies all the variations repeated on time scales less than a year, including the prominent semi-annual oscillation (SAO). Further, we calculated residual (de-seasonalized) amplitudes by subtracting the composite daily mean from the daily estimates, and used the residuals to investigate long-term modulations of the tides.

4 Results and Discussion

This study is focused on estimating and investigating short-term, seasonal or intra-annual, long-term, and climatological variations in migrating diurnal DW1 (1,1) and semidiurnal SW2 (2,2) and (2,3) tidal modes utilizing TIDI/TIMED MLT wind observations from 2002 to 2016. In addition, we estimate day-to-day tidal variability in these modes using fully sampled 2010 assimilated winds from NAVGEM-HA and HWM14 and compare them with the tidal estimates from TIDI. HWM14 is a climatological model, hence short-term variations are not expected in the HWM14 results.

Figure 2 illustrates the direct comparison between the tidal estimates determined using 2010 TIDI, NAVGEM-HA, and HWM14 meridional wind data. Both the DW1 and SW2 modes from TIDI and NAVGEM-HA exhibit significant short-term and seasonal variability. The overall morphologies of the tidal estimates from TIDI, NAVGEM-HA, and HWM14 are in agreement, except for SW2 (2,2) phase between days 130 and 210. The tidal morphology shown in Figure 2 is representative of the known seasonal character of the tides. Overall, the seasonal variability computed from HWM14 for DW1 and SW2 modes also agree with TIDI and NAVGEM-HA, except for SW2 (2,2) phase. The estimated diurnal and semidiurnal tidal amplitudes exhibit short-term variability ranging from days to weeks. The daily tidal amplitudes can be significantly greater or smaller than the mean (HWM14) profile. Although there are some discrepancies in the day-to-day variability of DW1 computed from TIDI and NAVGEM-HA, the short-term variations are very similar. In the case of SW2, the fitted results for both TIDI and NAVGEM-HA are scattered; nevertheless, the estimated SW2 exhibits similar short-term and seasonal modulation. The agreement between TIDI and NAVGEM-HA is better in the case of DW1 than in the case of SW2, for both the amplitudes and phases. It is important to note that, because of the way the data are fit, these tidal estimates are representative of the variability over a broad range of latitudes selected here. The local-time coverage of TIDI data over short periods of time is very limited. On the other hand, NAVGEM-HA and HWM14 wind fields are fully resolved in time and space. An overall good agreement between TIDI, NAVGEM-HA, and HWM14 results shown in Figure 2 on various time scales endorses the Hough mode analysis used. The underlying causes of disagreement between TIDI and NAVGEM-HA estimates require further study.

The tidal estimates for each year including 2010 are shown in Figures S3 to S8 (in supplementary information). These figures highlight the stable mean seasonal modulation of diurnal and semidiurnal tides and the pervasive short-term variations. Figure 3 shows tidal amplitudes and phases from year 2002 to 2016. Overpotted in red are composite daily means as a function of day of year calculated by averaging amplitude and phases from 2002 to 2016. Figure 3 is produced to obtain a climatological perspective of DW1 and SW2 tides, whereas supporting information Figures S3 to S8 illustrate similar information but from a long-term, time-dependent perspective. The mean morphology of the climatology shown in Figure 3 matches with documented behavior of the tides [e.g., *Burrage et al.*, 1995; *Xu et al.*, 2009; *Davis et al.*, 2013]. . The estimated DW1 tidal amplitudes show semiannual seasonal behavior with maxima occurring in equinox and minima in solstice, whereas semiannual behavior is not apparent in SW2 because of a maximum occurring in the summer season too. As depicted in Figure 3, the annual structure of both DW1 and SW2 is consistent from year to year; the short-term tidal estimates appear to form an envelope around the mean tidal variability. These figures (3, S3 to S8) clearly illustrate tidal variations from year to year on the same composite day.

An interesting feature in the 2010 DW1 amplitude (Figure 2) is the steep dip between day number 60 and 90. TIDI and NAVGEM-HA both show very similar dips in DW1 amplitude around the same time period. This dip is ~26m/s (64%) lower than the climatological amplitude estimated by HWM14. Similar dips in amplitude around the same time of year are present in multiple other years (refer to Figure S3). In addition, SW2 (2,2) and (2,3) modes (Figure S2) in the southern hemisphere show a similar steep dip between day number 60 and 90. No such feature is present the northern hemisphere SW2 modes (Figure 2). The short-term variability in diurnal MLT tide in temperature in 2009 at the equator, estimated by *Nguyen and Palo* [2013] (by combining temperature measurements from AURA MLS and TIMED SABER) also suggests the presence of a dip in amplitude around the same time period. Also, the phase of the diurnal tide calculated in *Nguyen and Palo* [2013] matches very well with the phase estimated here. The overall morphology of the equatorial diurnal tide in temperature presented in *Nguyen and Palo* [2013] agrees well with the diurnal tide presented in Figure S3. Even though a similar dip is present in a few other years, it is much more prominent in 2010.

In the 2010 DW1 (Figure 2), there are changes in phase of almost ~8hr in January and July-August. Such short-term phase variability is washed out in the climatology. As shown in Figure 3, the average DW1 phase moves to later local times in the solstices, compared to equinox.

Because of the presence of intra-annual variations in the tidal amplitudes, it is difficult to find any long-term variation directly from the estimated tidal amplitudes (shown in Figures S3, S5, and S7). Therefore, we de-seasonalized the amplitudes (i.e. calculated residuals) by subtracting the composite daily mean (shown in red in Figure 3) from the tidal estimates. This removes any annually repeated variations from the tidal amplitudes and yields a dataset of perturbations around the annual mean behavior. The calculated deseasonalized amplitudes for DW1 and SW2 modes as a function of year and day of year are illustrated in Figure 4. In this figure, the y-axis presents the intra-annual variation and the x-axis represents the inter-annual variability.

DW1 amplitude residuals shown in Figure 4 indicate the presence of biennial oscillations. Past modeling and observational studies [e.g., *Hagan et al.*, 1999, and herein] suggests that such oscillations are most likely the signature of the QBO modulation of tides. As shown in Figure 4, from years 2002 to 2009, the biennial behavior of DW1 in equinoxes and solstices is fairly consistent across all seasons, suggesting a square-wave-like variation. However, after 2009, the seasonal signature of the biennial behavior has changed; spring equinox (day number 60-100) and fall equinox (day number 230-290) amplitude residual variations are apparently out of phase. On the other hand, biennial oscillations are not apparent in SW2 modes.

To better illustrate the biennial oscillations in tides and their teleconnection with stratospheric QBO, we compared the mean spring equinox amplitude residuals with fall equinox residuals each year as shown in Figure 5. In addition, this figure (bottom panel) shows the stratospheric QBO in equatorial March and September mean stratospheric zonal winds from 2002 to 2016 at 30hPa from the Singapore radiosonde station. The biennial oscillations in DW1 are much more apparent in the equinoctial residual time series shown in Figure 5, indicating that their underlying cause is prominent when vertical propagation and growth of DW1 is most pronounced. The residual DW1 amplitudes in fall and spring equinoxes track each other until 2009, and are out of phase thereafter. The biennial oscillations in the March/September mean DW1 are similar to the March/September mean stratospheric zonal winds, which suggests that the biennial oscillations in DW1 are connected to the QBO (i.e., QBO modulation of DW1 tide). Even though there is no signature of a biennial oscillation in SW2 modes as shown in Figure 4, we applied the above discussed procedure also on SW2 residuals. Interestingly, the biennial oscillations are evident at least in the Spring equinox SW2 residual amplitudes (Figure 5), but they are less apparent than DW1. Variation in the SW2 (both modes) spring equinox correlates with the March QBO until 2013; after that their variation is opposite. On the other hand, a biennial oscillation is apparent in SW2 Fall equinox after 2012 and matches the phase of the September QBO.

The DW1 March mean amplitude varies between 26 m/s and 54 m/s with an average of 37 m/s. This variation in September is between 16 m/s and 50 m/s with an average of 32 m/s. Similarly, March mean amplitude for SW2 (2,2) (and (2,3)) varies between 32 m/s (32 m/s) and 112 m/s (68 m/s) with an average of 60 m/s (55 m/s). This variation in September is between 28 m/s (30 m/s) and 56 m/s (61 m/s) with an average of 43 m/s (45 m/s). The spring equinox tides are stronger than the fall equinox tides. The inter-annual standard deviation of the DW1 residual amplitude in the spring and fall equinoxes before QBO disruption (2003-2014) are ~9 m/s and 6 m/s respectively. These numbers for SW2 (2,2) (and (2,3)) mode are ~9 m/s (9 m/s) and ~9 m/s (9 m/s). The large SW2 residual amplitudes in 2002 as shown in Figure 5 may be associated with the larger LOS wind errors in the beginning phase of the TIDI observations.

Earlier studies of long-term variations in MLT migrating diurnal tides have found no statistically significant correlation between tidal amplitude and solar activity [e.g., *Fraser et al.*, 1989; *Bremer et al.*, 1997]. Recently, *Singh and Gurubaran* [2017] studied solar cycle variation of the diurnal tide using ground-based MF radar located at Tirunelveli (8.7°N, 77.8°E), TIDI, and SABER measurements;the ground-based tides suggested a prominent solar cycle variation, but the space-based tides showed no clear solar cycle dependence. The solar control of semidiurnal tides has also been proposed several times, but there is no consensus on the expected direction of the dependence. Studies such as *Sprenger and Schminder* [1969]; *Greisiger et al.* [1987]; *Namboothiri et al.* [1993, 1994] reported negative solar-cycle dependence, while *Jacobi et al.* [1997] reported positive solar-cycle dependence. *Fraser et al.* [1989] and *Fraser* [1990] found no clear evidence of their solar control. The statistical significance of these correlations discussed in above studies is generally low. Our study covers the second half of solar cycle 23 and slightly more than the first half of solar cycle 24 and includes the deep solar minimum of 2008 and 2009. The diurnal and semidiurnal amplitudes calculated in this study thus allow us to revisit the long-term and solar cycle dependence of tides.

The time series of de-seasonalized DW1 and SW2 mode amplitudes are illustrated in Figures 6a, 7a, and 8a. These figures (6, 7, and 8) also include annual mean and March mean amplitudes (shown in panel b) to better assist in investigating the long-term variations in tides. The inspection of DW1 residual amplitudes shows fluctuations correlated with QBO and no clear evidence of any solar cycle or long-term trend. The biennial behavior may be so strong that it is masking out any long-term or solar cycle variability. In addition, the DW1 annual and March mean amplitudes (Figure 6b) do not exhibit any

apparent long-term trend that can be associated with solar cycle. However, after 2009, both show a slight increase in amplitude. DW1 annual average increased by ~20 m/s between 2009 and 2016. In the case of SW2 (2,2), the residual (Figure 7a) and annual mean amplitudes (Figure 7b) show slight increases with time after 2003. No such signal is apparent in March mean amplitudes. The variability in SW2 (2,2) tidal estimates is so large that the overall increase in the SW2 (2,2) annual mean amplitude is insignificant as shown in Figure 7b. Similarly, in the case of SW2 (2,3) mode (Figure 8), there is no apparent variability associated with the solar cycle. Therefore, from these results, we find no evidence of solar cycle or long-term variability in either DW1 or SW2 tides, over the period studied in this report. Further study would benefit from including the UARS HRDI and WINDII datasets and to continue monitoring TIDI dataflow into Solar Cycle 25.

To statistically analyze and quantify the short-term variability in DW1 and SW2 modes, we make use of the residuals show in Figures 6a, 7a, and 8a and create histograms of the residuals as shown in Figures 6c, 7c, and 8c. The standard deviations around the mean for DW1, SW2 (2,2), and SW2 (2,3) are ~9 m/s, 33 m/s, and 20 m/s, respectively. However, as shown in Figure 5 there is significant interannual variability. Therefore, to isolate only the short-term variability (less than 60 days) from de-seasonalized amplitudes, we calculated a 60-day running mean and subtracted it from the residuals calculated earlier. The histograms of the resulting quantities for DW1 and SW2 modes are shown in Figures 6d, 7d, and 8d. The calculated standard deviation of the resulting quantities for DW1, SW2 (2,2), and SW2 (2,3) are ~7 m/s, 30 m/s, and 18 m/s, respectively.

5 Conclusions

This study is focused on estimating short-term, seasonal, long-term, and climatological variations of the MLT region migrating diurnal DW1 ((1,1) mode) and semidiurnal tides SW2 ((2,2) and (2,3) modes) utilizing the extensive archive of TIMED/TIDI meridional wind measurements together with fully resolved fields from NAVGEM-HA and HWM14. Here, we utilize the TIDI MLT meridional wind measurements and exploit the physical constraint of Hough functions to estimate the variability in migrating diurnal DW1 (westward, wave number 1 – (1,1) mode) and migrating semidiurnal SW2 (westward, wave number 2 – (2,2) and (2,3) modes) tides on various time scales. All three data sets included in this study are self-contained; therefore, the tidal parameters estimated from them are independent of each other.

Both DW1 and SW2 estimated from TIDI and NAVGEM-HA exhibit short-term, seasonal, and long-term variability. The mean tidal features in 2010 are representative of the seasonal features of the tides documented in the literature. Although there are minor discrepancies in the tides computed from TIDI and NAVGEM-HA, the tidal morphologies are similar on short-term and seasonal time scales. HWM14 tidal estimates also show very similar seasonal variations, except in the SW2 (2,2) phase. The agreement between TIDI, NAVGEM-HA, and HWM14 is better for DW1 than SW2. Also, there are pronounced variations in DW1 and SW2 on seasonal and inter-annual time scales. The remaining differences between the amplitudes of the migrating tides observed in the synoptic wind observations by the TIDI instrument and inferred by the NAVGEM-HA model from tropospheric meteorology and satellite temperature measurements require further investigation.

An interesting feature in the 2010 DW1 tide calculated from TIDI and NAVGEM-HA is the dip of ~26 m/s in the winter maximum between day number 60 and 90. This is a ~64% decrease in amplitude as compared to the climatological average from HWM14. Similar features around the same time period are present in multiple other years. The DW1 phase moves to later local times in the solstices, compared to equinox. There are some strong changes in the phase of almost ~8 hr in January and July-August months. Both TIDI and NAVGEM-HA data sets reflect similar significant short-term tidal variabil-

ity in tides that is not apparent in HWM14 climatology. The short-term tidal amplitudes can be greater or smaller than the mean profile, forming an envelope around the mean tidal variability. Statistical analyses of the de-seasonalized amplitudes using 15 years of TIDI data suggest that the short-term, 1-sigma variability in DW1, SW2 (2,2), and SW2 (2,3) is of the order of ~9 m/s, 33 m/s, and 20 m/s, respectively.

The de-seasonalized amplitudes of DW1 and SW2 modes also show biennial oscillations. The oscillations in DW1 and SW2 modes appear similar to the equatorial QBO in stratospheric zonal winds suggesting QBO modulation of tides. The QBO associated variations are more apparent in DW1 than SW2 modes. Variation in SW2 (both modes) spring equinox match well with the March QBO until 2013; after that their variation is opposite. The biennial oscillation is apparent in SW2 Fall equinox after 2012 and matches well with September QBO. The inter-annual standard deviation of DW1 residual amplitudes in spring and fall equinoxes (2003-2014) before QBO disruption are ~9 m/s and 6 m/s respectively. These numbers for SW2 (2,2) (and (2,3)) are ~9 m/s (9 m/s) and ~9 m/s (9 m/s).

Although long-term analysis of DW1 de-seasonalized amplitudes shows fluctuations correlated with stratospheric QBO, there is no clear evidence of solar cycle dependence. The biennial behavior in DW1 amplitudes may be so strong that it is masking out any solar cycle associated variability. However, after 2009, average annual DW1 amplitude shows an increase of ~20 m/s from 2009 to 2016. The de-seasonalized amplitudes of SW2 (2,2) mode show a slight increase in time after 2003. SW2 (2,3) mode de-seasonalized amplitudes show no variations associated with solar cycle. Therefore, from this analysis, we find no evidence of long-term variability in DW1 and SW2 modes.

As the migrating diurnal and semidiurnal tides propagate vertically, away from the source regions in the troposphere and stratosphere, they can be impacted by a number of factors which can modify their amplitude and phase. In the future, we plan to study the mechanisms that contribute to the short-term variability in tides. Migrating diurnal and semidiurnal tides are a prominent mode of energetic and dynamical coupling between the MLT and the upper thermosphere and ionosphere. Further studies, both theoretical and observational are therefore desirable to understand the contribution of tidal variability to many ionospheric and thermospheric properties.

Acknowledgments

This study was supported by NASA's Heliophysics Supporting Research Program (grant NNH16AC38I). This work was conducted while Manbharat Singh Dhadly held a National Research Council's Research Associateship at Naval Research Laboratory, Washington, DC. TIDI operations are supported by NASA grant NNX14AC82G. TIDI level 3 vector winds can be available at `ftp://tidi.engin.umich.edu/tidi/vector/`. NAVGEM-HA winds used in this study can be accessed at `https://map.nrl.navy.mil/map/pub/nrl/navgem/`. Singapore stratospheric winds can be accessed at `http://www.geo.fu-berlin.de/en/met/ag/strat/produkte/qbo/`. Current Horizontal Wind Model is available at `https:/map.nrl.navy.mil/map/pub/nrl/HWM/HWM14/` and as supplemental information in *Drob et al.* [2015].

References

Andrews, D. G., J. R. Holton, and C. B. Leovy (1987), *Middle atmosphere dynamics*, 489 pp., Academic Press.

Beard, A., N. Mitchell, P. Williams, and M. Kunitake (1999), Non-linear interactions between tides and planetary waves resulting in periodic tidal variability, *J. Atmos. Solar-Terrestrial Phys.*, *61*(5), 363–376, doi:10.1016/S1364-6826(99)00003-6.

Beldon, C. L., and N. J. Mitchell (2010), Gravity wave-tidal interactions in the mesosphere and lower thermosphere over Rothera, Antarctica (68řS, 68řW), *J. Geophys. Res.*, *115*(D18), D18,101, doi:10.1029/2009JD013617.

Bremer, J., R. Schminder, K. M. Greisiger, P. Hoffmann, D. Kürschner, and W. Singer (1997), Solar cycle dependence and long-term trends in the wind field of the mesosphere/lower thermosphere, *J. Atmos. Solar-Terrestrial Phys.*, *59*(5), 497–509, doi: https://doi.org/10.1016/S1364-6826(96)00032-6.

Buriti, R. A., W. K. Hocking, P. P. Batista, A. F. Medeiros, and B. R. Clemesha (2008), Observations of equatorial mesospheric winds over Cariri (7.4° S) by a meteor radar and comparison with existing models, *Ann. Geophys.*, *26*(3), 485–497, doi: 10.5194/angeo-26-485-2008.

Burrage, M. D., M. E. Hagan, W. R. Skinner, D. L. Wu, and P. B. Hays (1995), Long-term variability in the solar diurnal tide observed by HRDI and simulated by the GSWM, *Geophys. Res. Lett.*, *22*(19), 2641–2644, doi:10.1029/95GL02635.

Chang, J. L., and S. K. Avery (1997), Observations of the diurnal tide in the mesosphere and lower thermosphere over Christmas Island, *J. Geophys. Res. Atmos.*, *102*(D2), 1895–1907, doi:10.1029/96JD03378.

Chang, L. C., S. E. Palo, and H.-L. Liu (2011), Short-term variability in the migrating diurnal tide caused by interactions with the quasi 2 day wave, *J. Geophys. Res.*, *116*(D12), D12,112, doi:10.1029/2010JD014996.

Chapman, S., and R. S. Lindzen (1970), *Atmospheric tides : thermal and gravitational*, 212 pp., D. Reidel.

Davis, R. N., J. Du, A. K. Smith, W. E. Ward, and N. J. Mitchell (2013), The diurnal and semidiurnal tides over Ascension Island (8S,14W) and their interaction with the stratospheric quasi-biennial oscillation: studies with meteor radar, eCMAM and WACCM, *Atmos. Chem. Phys.*, *13*(18), 9543–9564, doi:10.5194/acp-13-9543-2013.

Drob, D. P., J. T. Emmert, J. W. Meriwether, J. J. Makela, E. Doornbos, M. Conde, G. Hernandez, J. Noto, K. A. Zawdie, S. E. McDonald, J. D. Huba, and J. H. Klenzing (2015), An update to the Horizontal Wind Model (HWM): The quiet time thermosphere, *Earth Sp. Sci.*, *2*, doi:10.1002/2014EA000089.

England, S. L., S. Maus, T. J. Immel, and S. B. Mende (2006), Longitudinal variation of the E-region electric fields caused by atmospheric tides, *Geophys. Res. Lett.*, *33*(21), L21,105, doi:10.1029/2006GL027465.

Fang, T.-W., R. Akmaev, T. Fuller-Rowell, F. Wu, N. Maruyama, and G. Millward (2013), Longitudinal and day-to-day variability in the ionosphere from lower atmosphere tidal forcing, *Geophys. Res. Lett.*, *40*(11), 2523–2528, doi:10.1002/grl.50550.

Fiedler, J., G. Baumgarten, and G. von Cossart (2005), Mean diurnal variations of noctilucent clouds during 7 years of lidar observations at ALOMAR, *Ann. Geophys.*, *23*(4), 1175–1181, doi:10.5194/angeo-23-1175-2005.

Forbes, J. M. (1982a), Atmospheric tides: 1. Model description and results for the solar diurnal component, *J. Geophys. Res.*, *87*(1), 5222–5240, doi:10.1029/JA087iA07p05222.

Forbes, J. M. (1982b), Atmospheric tide: 2. The solar and lunar semidiurnal components, *J. Geophys. Res. Sp. Phys.*, *87*(A7), 5241–5252, doi:10.1029/JA087iA07p05241.

Forbes, J. M. (1995), Tidal and Planetary Waves: The upper mesosphere and lower thermosphere: A review of experiment and theory, in *Geophys. Monogr. Ser.*, pp. 67–87, American Geophysical Union, doi:10.1029/GM087p0067.

Forbes, J. M. (2009), Vertical coupling by the semidiurnal tide in Earth's atmosphere, pp. 337–348.

Forbes, J. M., and H. B. Garrett (1979), Theoretical studies of atmospheric tides, *Rev. Geophys.*, *17*(8), 1951, doi:10.1029/RG017i008p01951.

Forbes, J. M., and G. V. Groves (1987), Diurnal propagating tides in the low-latitude middle atmosphere, *J. Atmos. Terr. Phys.*, *49*(2), 153–164, doi:10.1016/0021-9169(87)90050-X.

Forbes, J. M., and M. E. Hagan (1982), Thermospheric extensions of the classical expansion functions for semidiurnal tides, *J. Geophys. Res. Sp. Phys.*, *87*(A7), 5253–5259, doi:10.1029/JA087iA07p05253.

Forbes, J. M., H. B. Garrett, J. M. Forbes, and H. B. Garrett (1976), Solar Diurnal Tide in the Thermosphere, *J. Atmos. Sci.*, *33*(11), 2226–2241, doi:10.1175/1520-0469(1976)033<2226:SDTITT>2.0.CO;2.

Forbes, J. M., S. E. Palo, and X. Zhang (2000), Variability of the ionosphere, *J. Atmos. Solar-Terrestrial Phys.*, *62*(8), 685–693, doi:10.1016/S1364-6826(00)00029-8.

Forbes, J. M., D. Wu, J. M. Forbes, and D. Wu (2006), Solar Tides as Revealed by Measurements of Mesosphere Temperature by the MLS Experiment on UARS, *J. Atmos. Sci.*, *63*(7), 1776–1797, doi:10.1175/JAS3724.1.

Forbes, J. M., X. Zhang, S. Palo, J. Russell, C. J. Mertens, and M. Mlynczak (2008), Tidal variability in the ionospheric dynamo region, *J. Geophys. Res. Sp. Phys.*, *113*(A2), doi:10.1029/2007JA012737.

Fraser, G. (1990), Long-term variations in mid-latitude southern hemisphere mesospheric winds, *Adv. Sp. Res.*, *10*(10), 247–250, doi:10.1016/0273-1177(90)90039-3.

Fraser, G. J., R. A. Vincent, A. H. Manson, C. E. Meek, and R. R. Clark (1989), Interannual variability of tides in the mesosphere and lower thermosphere, *J. Atmos. Terr. Phys.*, *51*(7), 555–567, doi:https://doi.org/10.1016/0021-9169(89)90054-8.

Friedman, J. S., X. Zhang, X. Chu, and J. M. Forbes (2009), Longitude variations of the solar semidiurnal tides in the mesosphere and lower thermosphere at low latitudes observed from ground and space, *J. Geophys. Res.*, *114*(D11), D11,114, doi:10.1029/2009JD011763.

Fritts, D. C., R. A. Vincent, D. C. Fritts, and R. A. Vincent (1987), Mesospheric Momentum Flux Studies at Adelaide, Australia: Observations and a Gravity Wave-Tidal Interaction Model, *J. Atmos. Sci.*, *44*(3), 605–619, doi:10.1175/1520-0469(1987)044<0605:MMFSAA>2.0.CO;2.

Goncharenko, L., J. L. Chau, P. Condor, A. Coster, and L. Benkevitch (2013), Ionospheric effects of sudden stratospheric warming during moderate-to-high solar activity: Case study of January 2013, *Geophys. Res. Lett.*, *40*(19), 4982–4986, doi:10.1002/grl.50980.

Greisiger, K. M., R. Schminder, and D. Kürschner (1987), Long-period variations of wind parameters in the mesopause region and the solar cycle dependence, *J. Atmos. Terr. Phys.*, *49*(3), 281–285, doi:https://doi.org/10.1016/0021-9169(87)90063-8.

Gurubaran, S., R. Rajaram, T. Nakamura, T. Tsuda, D. Riggin, and R. A. Vincent (2009), Radar observations of the diurnal tide in the tropical mesosphere-lower thermosphere region: Longitudinal variabilities, *Earth, Planets Sp.*, *61*(4), 513–524, doi:10.1186/BF03353168.

Hagan, M. E., and J. M. Forbes (2003), Migrating and nonmigrating semidiurnal tides in the upper atmosphere excited by tropospheric latent heat release, *J. Geophys. Res. Sp. Phys.*, *108*(A2), doi:10.1029/2002JA009466.

Hagan, M. E., M. D. Burrage, J. M. Forbes, J. Hackney, W. J. Randel, and X. Zhang (1999), GSWM-98: Results for migrating solar tides, *J. Geophys. Res. Sp. Phys.*, *104*(A4), 6813–6827, doi:10.1029/1998JA900125.

Hagan, M. E., A. Maute, and R. G. Roble (2009), Tropospheric tidal effects on the middle and upper atmosphere, *J. Geophys. Res. Sp. Phys.*, *114*(A1), n/a–n/a, doi:10.1029/2008JA013637.

Hamilton, K., and K. Hamilton (1998), Effects of an Imposed Quasi-Biennial Oscillation in a Comprehensive Troposphere-Stratosphere-Mesosphere General Circulation Model, *J. Atmos. Sci.*, *55*(14), 2393–2418, doi:10.1175/1520-0469(1998)055<2393:EOAIQB>2.0.CO;2.

Häusler, K., and H. Luhr (2009), Nonmigrating tidal signals in the upper thermospheric zonal wind at equatorial latitudes as observed by CHAMP, *Ann. Geophys*, *27*, 2643–2652.

Hays, P. B., D. L. Wu, T. HRDI Science Team, P. B. Hays, D. L. Wu, and T. H. S. Team (1994), Observations of the Diurnal Tide from Space, *J. Atmos. Sci.*, *51*(20), 3077–3093, doi:10.1175/1520-0469(1994)051<3077:OOTDTF>2.0.CO;2.

Hernandez, G., G. J. Fraser, and R. W. Smith (1993), Mesospheric 12-hour oscillation near South Pole, Antarctica, *Geophys. Res. Lett.*, *20*(17), 1787–1790, doi:10.1029/93GL01983.

Hogan, T. F., M. Liu, J. A. Ridout, M. S. Peng, T. R. Whitcomb, B. C. Ruston, C. A. Reynolds, S. D. Eckermann, J. R. Moskaitis, N. L. Baker, J. P. Mccormack, K. C. Viner, J. G. Mclay, M. K. Flatau, L. Xu, C. Chen, and S. W. Chang (2014), The Navy Global Environmental Model, *Oceanography*, *27*, 116–125, doi:10.2307/24862194.

Huang, F. T., H. G. Mayr, C. A. Reber, J. M. Russell, M Mlynczak, and J. G. Mengel (2006), Stratospheric and mesospheric temperature variations for the quasi-biennial and semiannual (QBO and SAO) oscillations based on measurements from SABER (TIMED) and MLS (UARS), *Ann. Geophys.*, *24*(8), 2131–2149, doi:10.5194/angeo-24-2131-2006.

Immel, T. J., E. Sagawa, S. L. England, S. B. Henderson, M. E. Hagan, S. B. Mende, H. U. Frey, C. M. Swenson, and L. J. Paxton (2006), Control of equatorial ionospheric morphology by atmospheric tides, *Geophys. Res. Lett.*, *33*(15), L15,108, doi:10.1029/2006GL026161.

Jacobi, C., R. Schminder, D. Kürschner, J. Bremer, K. Greisiger, P. Hoffmann, and W. Singer (1997), Long-term trends in the mesopause wind field obtained from LF D1 wind measurements at Collm, Germany, *Adv. Sp. Res.*, *20*(11), 2085–2088, doi:10.1016/S0273-1177(97)00599-1.

Jacobi, C., Y. Portnyagin, T. Solovjova, P. Hoffmann, W. Singer, A. Fahrutdinova, R. Ishmuratov, A. Beard, N. Mitchell, H. Muller, R. Schminder, D. Kürschner, A. Manson, and C. Meek (1999), Climatology of the semidiurnal tide at 52-56ř̌N from ground-based radar wind measurements 1985-1995, *J. Atmos. Solar-Terrestrial Phys.*, *61*(13), 975–991, doi:10.1016/S1364-6826(99)00065-6.

Jin, H., Y. Miyoshi, D. Pancheva, P. Mukhtarov, H. Fujiwara, and H. Shinagawa (2012), Response of migrating tides to the stratospheric sudden warming in 2009 and their effects on the ionosphere studied by a whole atmosphere-ionosphere model GAIA with COSMIC and TIMED/SABER observations, *J. Geophys. Res. Sp. Phys.*, *117*(A10), A10,323, doi:10.1029/2012JA017650.

Killeen, T. L., W. R. Skinner, R. M. Johnson, C. J. Edmonson, Q. Wu, R. J. Niciejewski, H. J. Grassl, D. A. Gell, P. E. Hansen, J. D. Harvey, and J. F. Kafkalidis (1999), TIMED Doppler interferometer (TIDI), p. 289, International Society for Optics and Photonics, doi:10.1117/12.366383.

Killeen, T. L., Q. Wu, S. C. Solomon, D. A. Ortland, W. R. Skinner, R. J. Niciejewski, and D. A. Gell (2006), TIMED Doppler Interferometer: Overview and recent results, *J. Geophys. Res.*, *111*(A10), A10S01, doi:10.1029/2005JA011484.

Kuhl, D. D., T. E. Rosmond, C. H. Bishop, J. McLay, N. L. Baker, D. D. Kuhl, T. E. Rosmond, C. H. Bishop, J. McLay, and N. L. Baker (2013), Comparison of Hybrid Ensemble/4DVar and 4DVar within the NAVDAS-AR Data Assimilation Framework, *Mon. Weather Rev.*, *141*(8), 2740–2758, doi:10.1175/MWR-D-12-00182.1.

Kumar, K. K., V. Deepa, T. M. Antonita, and G. Ramkumar (2008), Meteor radar observations of short-term tidal variabilities in the low-latitude mesosphere-lower thermosphere: Evidence for nonlinear wave-wave interactions, *J. Geophys. Res. Atmos.*, *113*(16), D16,108, doi:10.1029/2007JD009610.

Laskar, F. I., J. L. Chau, G. Stober, P. Hoffmann, C. M. Hall, and M. Tsutsumi (2016), Quasi-biennial oscillation modulation of the middle- and high-latitude mesospheric semidiurnal tides during August-September, *J. Geophys. Res. Sp. Phys.*, *121*(5), 4869–4879, doi:10.1002/2015JA022065.

Lieberman, R. S. (1997), Long-term variations of zonal mean winds and (1,1) driving in the equatorial lower thermosphere, *J. Atmos. Solar-Terrestrial Phys.*, *59*(13), 1483–1490,

doi:10.1016/S1364-6826(96)00150-2.

Lieberman, R. S., P. B. Hays, R. S. Lieberman, and P. B. Hays (1994), An Estimate of the Momentum Deposition in the Lower Thermosphere by the Observed Diurnal Tide, *J. Atmos. Sci.*, *51*(20), 3094–3105, doi:10.1175/1520-0469(1994)051<3094:AEOTMD>2.0.CO;2.

Lindzen, R. S., and S. Chapman (1979), Atmospheric Tides, *Annu. Rev. Earth Planet. Sci.*, *7*(1), 199–225, doi:10.1146/annurev.ea.07.050179.001215.

Lindzen, R. S., S. S. Hong, and J. M. Forbes (1977), Semidiurnal Hough Mode Extensions in the Thermosphere and Their Application, *Memo. Rep. 3442*, pp. Nav. Res. Lab., Washington, D.C.

Liu, H., E. Doornbos, and J. Nakashima (2016), Thermospheric wind observed by GOCE: Wind jets and seasonal variations, *J. Geophys. Res. Sp. Phys.*, *121*(7), 6901–6913, doi:10.1002/2016JA022938.

Mayr, H. G., and J. G. Mengel (2005), Interannual variations of the diurnal tide in the mesosphere generated by the quasi-biennial oscillation, *J. Geophys. Res.*, *110*(D10), D10,111, doi:10.1029/2004JD005055.

McCormack, J., K. Hoppel, D. Kuhl, R. de Wit, G. Stober, P. Espy, N. Baker, P. Brown, D. Fritts, C. Jacobi, D. Janches, N. Mitchell, B. Ruston, S. Swadley, K. Viner, T. Whitcomb, and R. Hibbins (2017), Comparison of mesospheric winds from a high-altitude meteorological analysis system and meteor radar observations during the boreal winters of 2009-2010 and 2012-2013, *J. Atmos. Solar-Terrestrial Phys.*, *154*, 132–166, doi:10.1016/j.jastp.2016.12.007.

McCormack, J. P., L. Coy, and W. Singer (2014), Intraseasonal and interannual variability of the quasi 2 day wave in the Northern Hemisphere summer mesosphere, *J. Geophys. Res. Atmos.*, *119*(6), 2928–2946, doi:10.1002/2013JD020199.

Mendillo, M., H. Rishbeth, R. Roble, and J. Wroten (2002), Modelling F2-layer seasonal trends and day-to-day variability driven by coupling with the lower atmosphere, *J. Atmos. Solar-Terrestrial Phys.*, *64*(18), 1911–1931, doi:10.1016/S1364-6826(02)00193-1.

Millward, G. H., I. C. F. Müller-Wodarg, A. D. Aylward, T. J. Fuller-Rowell, A. D. Richmond, and R. J. Moffett (2001), An investigation into the influence of tidal forcing on F region equatorial vertical ion drift using a global ionosphere-thermosphere model with coupled electrodynamics, *J. Geophys. Res. Sp. Phys.*, *106*(A11), 24,733–24,744, doi:10.1029/2000JA000342.

Mukhtarov, P., D. Pancheva, and B. Andonov (2009), Global structure and seasonal and interannual variability of the migrating diurnal tide seen in the SABER/TIMED temperatures between 20 and 120 km, *J. Geophys. Res. Sp. Phys.*, *114*(A2), A02,309, doi:10.1029/2008JA013759.

Namboothiri, S., A. Manson, and C. Meek (1993), Variations of mean winds and tides in the upper middle atmosphere over a solar cycle, Saskatoon, Canada, 52řN, 107řW, *J. Atmos. Terr. Phys.*, *55*(10), 1325–1334, doi:10.1016/0021-9169(93)90101-4.

Namboothiri, S., C. Meek, and A. Manson (1994), Variations of mean winds and solar tides in the mesosphere and lower thermosphere over time scales ranging from 6 months to 11 yr: Saskatoon, 52řN, 107řW, *J. Atmos. Terr. Phys.*, *56*(10), 1313–1325, doi:10.1016/0021-9169(94)90069-8.

Nguyen, V., and S. Palo (2013), Technique to produce daily estimates of the migrating diurnal tide using TIMED/SABER and EOS Aura/MLS, *J. Atmos. Solar-Terrestrial Phys.*, *105-106*, 39–53, doi:10.1016/J.JASTP.2013.07.008.

Niciejewski, R., Q. Wu, W. Skinner, D. Gell, M. Cooper, A. Marshall, T. Killeen, S. Solomon, and D. Ortland (2006), TIMED Doppler Interferometer on the Thermosphere Ionosphere Mesosphere Energetics and Dynamics satellite: Data product overview, *J. Geophys. Res.*, *111*(A11), A11S90, doi:10.1029/2005JA011513.

Niciejewski, R. J., and T. L. Killeen (1995), Nocturnal observations of the semidiurnal tide at a midlatitude site, *J. Geophys. Res.*, *100*(D12), 25,855, doi:10.1029/95JD02729.

Oberheide, J., and J. M. Forbes (2008), Tidal propagation of deep tropical cloud signatures into the thermosphere from TIMED observations, *Geophys. Res. Lett.*, *35*(4), L04,816, doi:10.1029/2007GL032397.

Oberheide, J., M. E. Hagan, R. G. Roble, and D. Offermann (2002), Sources of nonmigrating tides in the tropical middle atmosphere, *J. Geophys. Res. Atmos.*, *107*(D21), ACL 6–1–ACL 6–14, doi:10.1029/2002JD002220.

Oberheide, J., Q. Wu, T. L. Killeen, M. E. Hagan, and R. G. Roble (2006), Diurnal nonmigrating tides from TIMED Doppler Interferometer wind data: Monthly climatologies and seasonal variations, *J. Geophys. Res.*, *111*(A10), A10S03, doi:10.1029/2005JA011491.

Oberheide, J., J. M. Forbes, K. Häusler, Q. Wu, and S. L. Bruinsma (2009), Tropospheric tides from 80 to 400 km: Propagation, interannual variability, and solar cycle effects, *J. Geophys. Res.*, *114*(D1), D00I05, doi:10.1029/2009JD012388.

Oberheide, J., J. M. Forbes, X. Zhang, and S. L. Bruinsma (2011), Climatology of upward propagating diurnal and semidiurnal tides in the thermosphere, *J. Geophys. Res. Sp. Phys.*, *116*(A11), doi:10.1029/2011JA016784.

Oberheide, J., K. Shiokawa, S. Gurubaran, W. E. Ward, H. Fujiwara, M. J. Kosch, J. J. Makela, and H. Takahashi (2015), The geospace response to variable inputs from the lower atmosphere: a review of the progress made by Task Group 4 of CAWSES-II, *Prog. Earth Planet. Sci.*, *2*(1), 2, doi:10.1186/s40645-014-0031-4.

Ortland, D. A. (2005), A Study of the Global Structure of the Migrating Diurnal Tide Using Generalized Hough Modes, *J. Atmos. Sci.*, *62*(8), 2684–2702, doi:10.1175/JAS3501.1.

Ortland, D. A. (2017), Daily estimates of the migrating tide and zonal mean temperature in the mesosphere and lower thermosphere derived from SABER data, *J. Geophys. Res. Atmos.*, *122*(7), 3754–3785, doi:10.1002/2016JD025573.

Pedatella, N. M., H.-L. Liu, and A. D. Richmond (2012), Atmospheric semidiurnal lunar tide climatology simulated by the Whole Atmosphere Community Climate Model, *J. Geophys. Res. Sp. Phys.*, *117*(A6), A06,327, doi:10.1029/2012JA017792.

Pedatella, N. M., A. D. Richmond, A. Maute, and H.-L. Liu (2016), Impact of semidiurnal tidal variability during SSWs on the mean state of the ionosphere and thermosphere, *J. Geophys. Res. Sp. Phys.*, *121*(8), 8077–8088, doi:10.1002/2016JA022910.

Riggin, D. M., and R. S. Lieberman (2013), Variability of the diurnal tide in the equatorial MLT, *J. Atmos. Solar-Terrestrial Phys.*, *102*, 198–206, doi:10.1016/j.jastp.2013.05.011.

Shepherd, G. G., G. Thuillier, Y.-M. Cho, M.-L. Duboin, W. F. J. Evans, W. A. Gault, C. Hersom, D. J. W. Kendall, C. Lathuillère, R. P. Lowe, I. C. McDade, Y. J. Rochon, M. G. Shepherd, B. H. Solheim, D.-Y. Wang, and W. E. Ward (2012), The Wind Imaging Interferometer (WINDII) on the Upper Atmosphere Research Satellite: A 20 year perspective, *Rev. Geophys.*, *50*(2), doi:10.1029/2012RG000390.

Singh, D., and S. Gurubaran (2017), Variability of diurnal tide in the MLT region over Tirunelveli (8.7řN), India: Consistency between ground- and space-based observations, *J. Geophys. Res. Atmos.*, *122*(5), 2696–2713, doi:10.1002/2016JD025910.

Sprenger, K., and R. Schminder (1969), Solar cycle dependence of winds in the lower ionosphere, *J. Atmos. Terr. Phys.*, *31*(1), 217–221, doi:10.1016/0021-9169(69)90100-7.

Sridharan, S., T. Tsuda, and S. Gurubaran (2010), Long-term tendencies in the mesosphere/lower thermosphere mean winds and tides as observed by medium-frequency radar at Tirunelveli (8.7řN, 77.8řE), *J. Geophys. Res.*, *115*(D8), D08,109, doi:10.1029/2008JD011609.

Truskowski, A. O., J. M. Forbes, X. Zhang, and S. E. Palo (2014), New perspectives on thermosphere tides: 1. Lower thermosphere spectra and seasonal-latitudinal structures, *Earth, Planets Sp.*, *66*(1), 136, doi:10.1186/s40623-014-0136-4.

Vincent, R. A., S. Kovalam, D. C. Fritts, and J. R. Isler (1998), Long-term MF radar observations of solar tides in the low-latitude mesosphere: Interannual variability and

comparisons with the GSWM, *J. Geophys. Res. Atmos.*, *103*(D8), 8667–8683, doi: 10.1029/98JD00482.

Wang, H., J. P. Boyd, and R. A. Akmaev (2016), On computation of Hough functions, *Geosci. Model Dev.*, *9*(4), 1477–1488, doi:10.5194/gmd-9-1477-2016.

Ward, W. E., J. Oberheide, L. P. Goncharenko, T. Nakamura, P. Hoffmann, W. Singer, L. C. Chang, J. Du, D.-Y. Wang, P. Batista, B. Clemesha, A. H. Manson, D. M. Riggin, C.-Y. She, T. Tsuda, and T. Yuan (2010), On the consistency of model, ground-based, and satellite observations of tidal signatures: Initial results from the CAWSES tidal campaigns, *J. Geophys. Res.*, *115*(D7), D07,107, doi:10.1029/2009JD012593.

Wu, Q., D. McEwen, W. Guo, R. Niciejewski, R. Roble, and Y.-I. Won (2008), Long-term thermospheric neutral wind observations over the northern polar cap, *J. Atmos. Solar-Terrestrial Phys.*, *70*(16), 2014–2030, doi:10.1016/j.jastp.2008.09.004.

Wu, Q., D. Ortland, S. Solomon, W. Skinner, and R. Niciejewski (2011), Global distribution, seasonal, and inter-annual variations of mesospheric semidiurnal tide observed by TIMED TIDI, *J. Atmos. Solar-Terrestrial Phys.*, *73*(17-18), 2482–2502, doi: 10.1016/J.JASTP.2011.08.007.

Xu, J., A. K. Smith, H.-L. Liu, W. Yuan, Q. Wu, G. Jiang, M. G. Mlynczak, J. M. Russell, and S. J. Franke (2009), Seasonal and quasi-biennial variations in the migrating diurnal tide observed by Thermosphere, Ionosphere, Mesosphere, Energetics and Dynamics (TIMED), *J. Geophys. Res.*, *114*(D13), D13,107, doi:10.1029/2008JD011298.

Yamazaki, Y., and A. D. Richmond (2013), A theory of ionospheric response to upward-propagating tides: Electrodynamic effects and tidal mixing effects, *J. Geophys. Res. Sp. Phys.*, *118*(9), 5891–5905, doi:10.1002/jgra.50487.

Yamazaki, Y., K. Häusler, and J. A. Wild (2016), Day-to-day variability of midlatitude ionospheric currents due to magnetospheric and lower atmospheric forcing, *J. Geophys. Res. Sp. Phys.*, *121*(7), 7067–7086, doi:10.1002/2016JA022817.

Yigit, E., and A. S. Medvedev (2015), Internal wave coupling processes in Earth's atmosphere, *Adv. Sp. Res.*, *55*(4), 983–1003, doi:10.1016/J.ASR.2014.11.020.

Yuan, T., H. Schmidt, C. Y. She, D. A. Krueger, and S. Reising (2008), Seasonal variations of semidiurnal tidal perturbations in mesopause region temperature and zonal and meridional winds above Fort Collins, Colorado (40.6řN, 105.1řW), *J. Geophys. Res.*, *113*(D20), D20,103, doi:10.1029/2007JD009687.

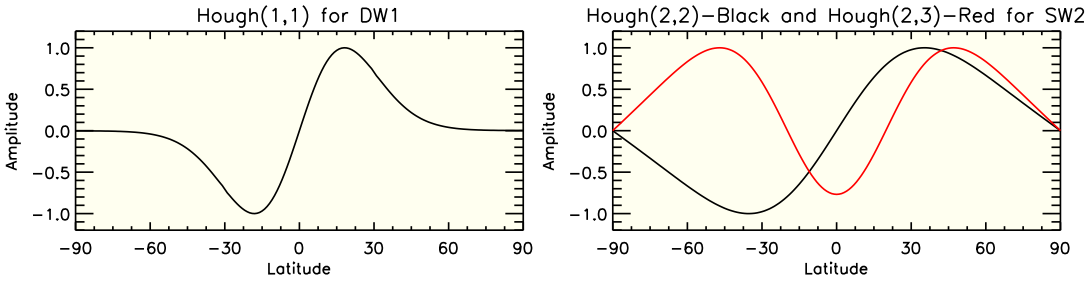

Figure 1. Normalized Hough functions for the diurnal (DW1, left panel) and semidiurnal (SW2, right panel) tidal components.

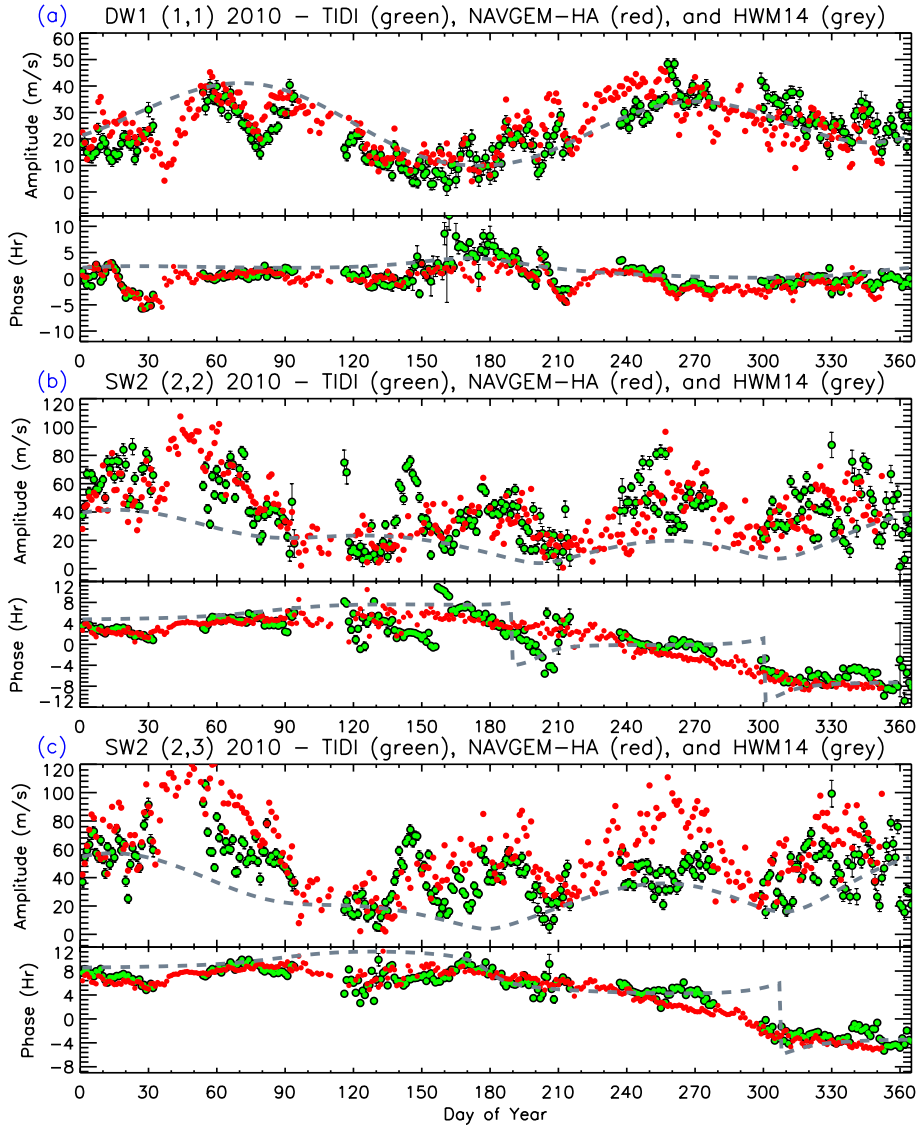

Figure 2. DW1 (1,1)(panel a), SW2 (2,2) (panel b), and SW2 (2,3) (panel c) tidal mode amplitudes and phases estimated from TIDI (green), NAVGEM-HA (red), and HWM14 (grey) meridional winds during 2010. Amplitude refers to maximum value, while phase refers to the local solar time of the maximum value. Error bars denote the $\pm 1\sigma$ uncertainty estimate. Note that SW2 (2,2) and (2,3) mode phases are wrapped to avoid unwanted discontinuities.

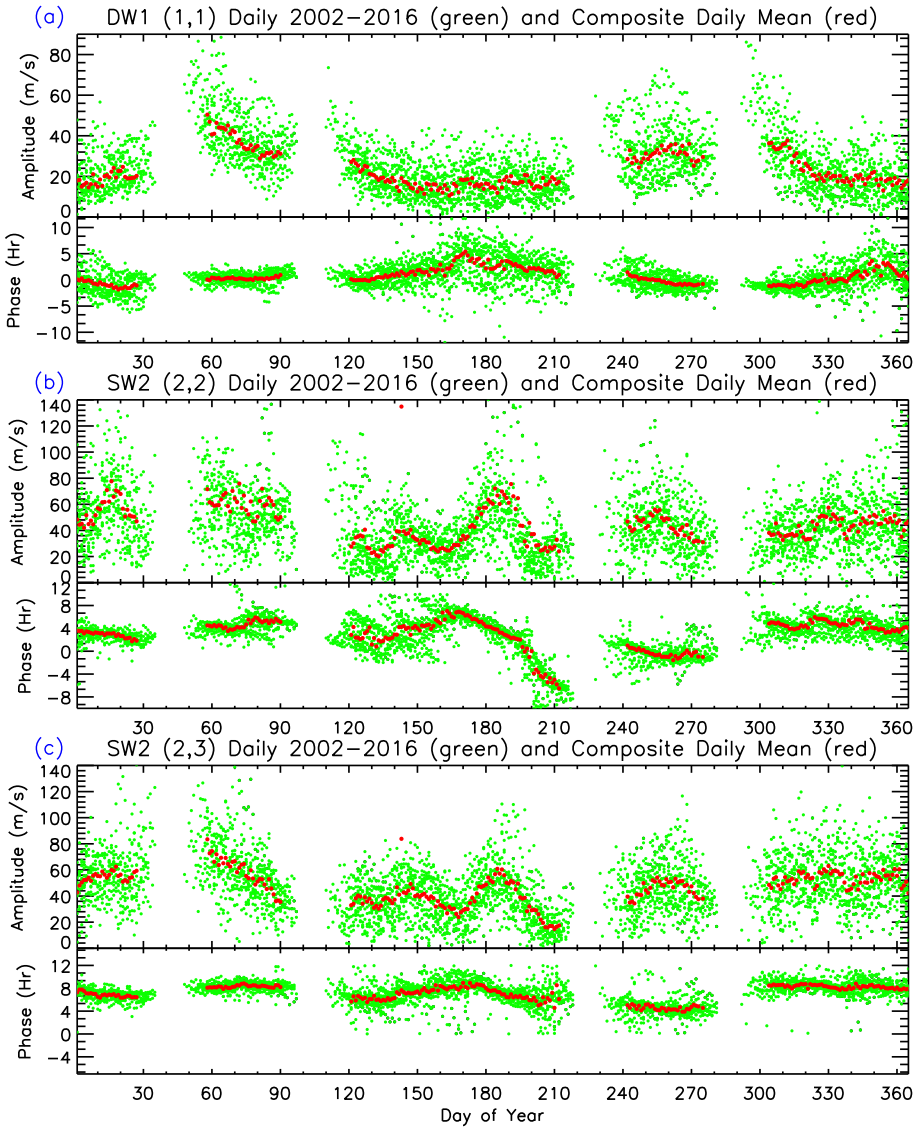

Figure 3. TIDI DW1 (1,1)(panel a), SW2 (2,2) (panel b), and SW2 (2,3) (panel c) daily and composite mean amplitudes and phases from 2002 to 2016. Note that SW2 (2,2) and (2,3) mode phases are wrapped to avoid unwanted discontinuities.

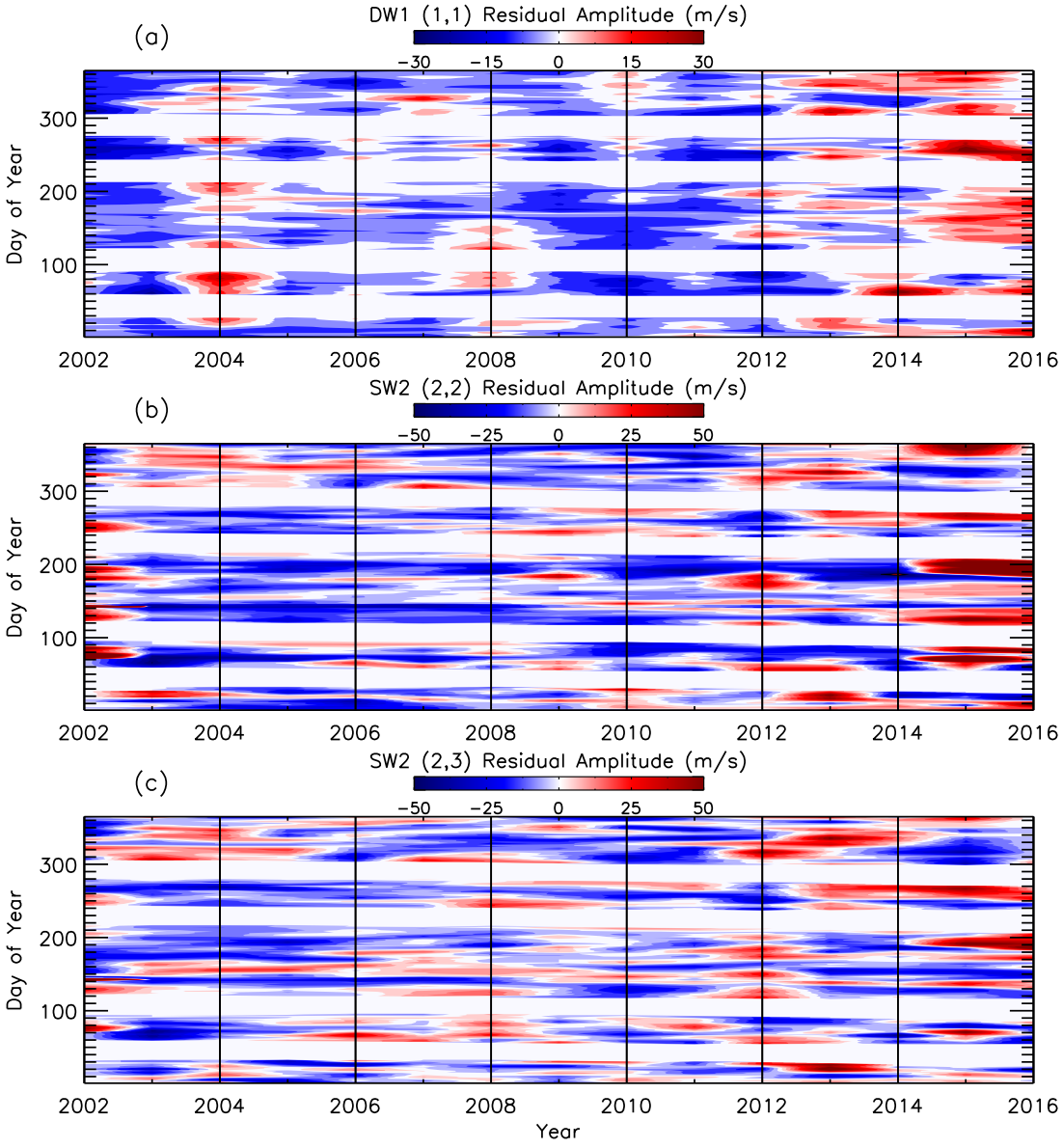

Figure 4. TIDI DW1 (1,1)(panel a), SW2 (2,2) (panel b), and SW2 (2,3) (panel c) residual amplitude (= daily amplitude - composite daily mean amplitude) contours as a function of year and day of year. Note that x-axis represent inter-annual variability and y-axis present intra-annual variability.

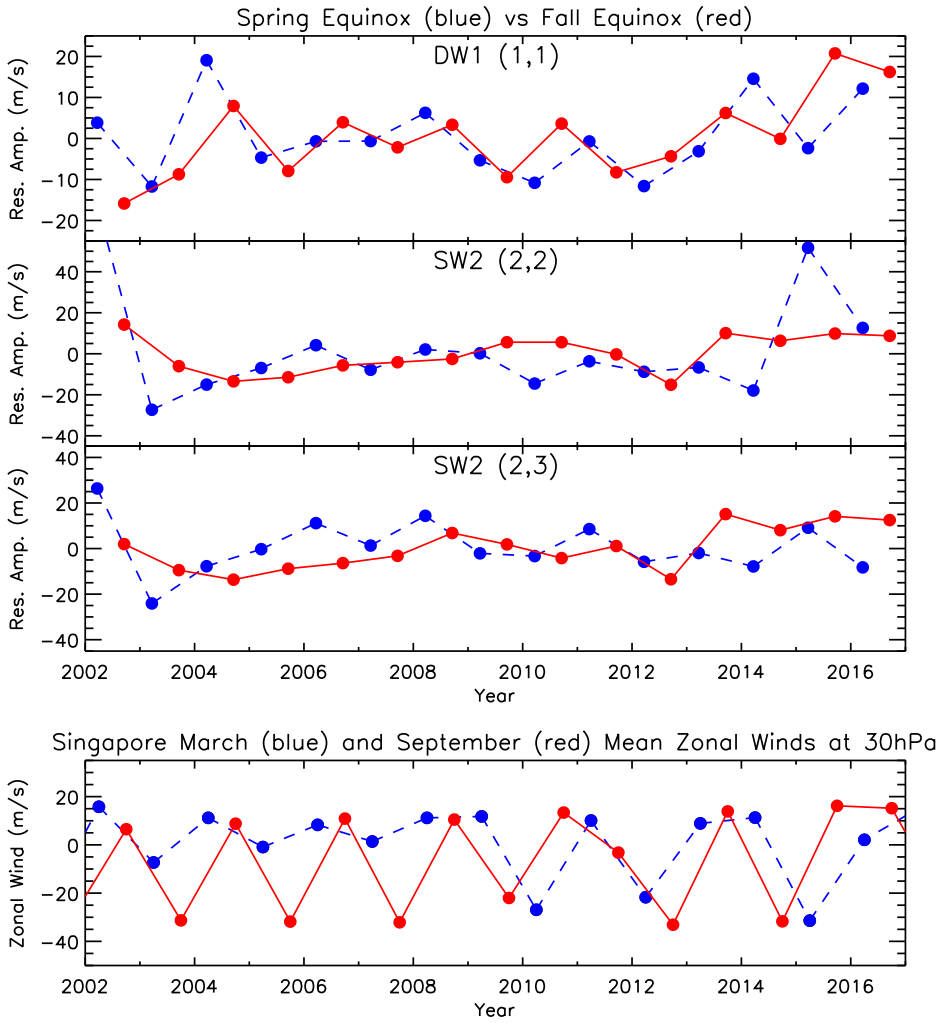

Figure 5. Top: comparison of TIDI DW1 (1,1), SW2 (2,2), and SW2 (2,3) mode amplitude residuals for spring equinox (day number 60-100, blue) and fall equinox (day number 230-290, red). Bottom: March (blue) and September (red) monthly mean stratospheric zonal winds at 30 hPa from Singapore.

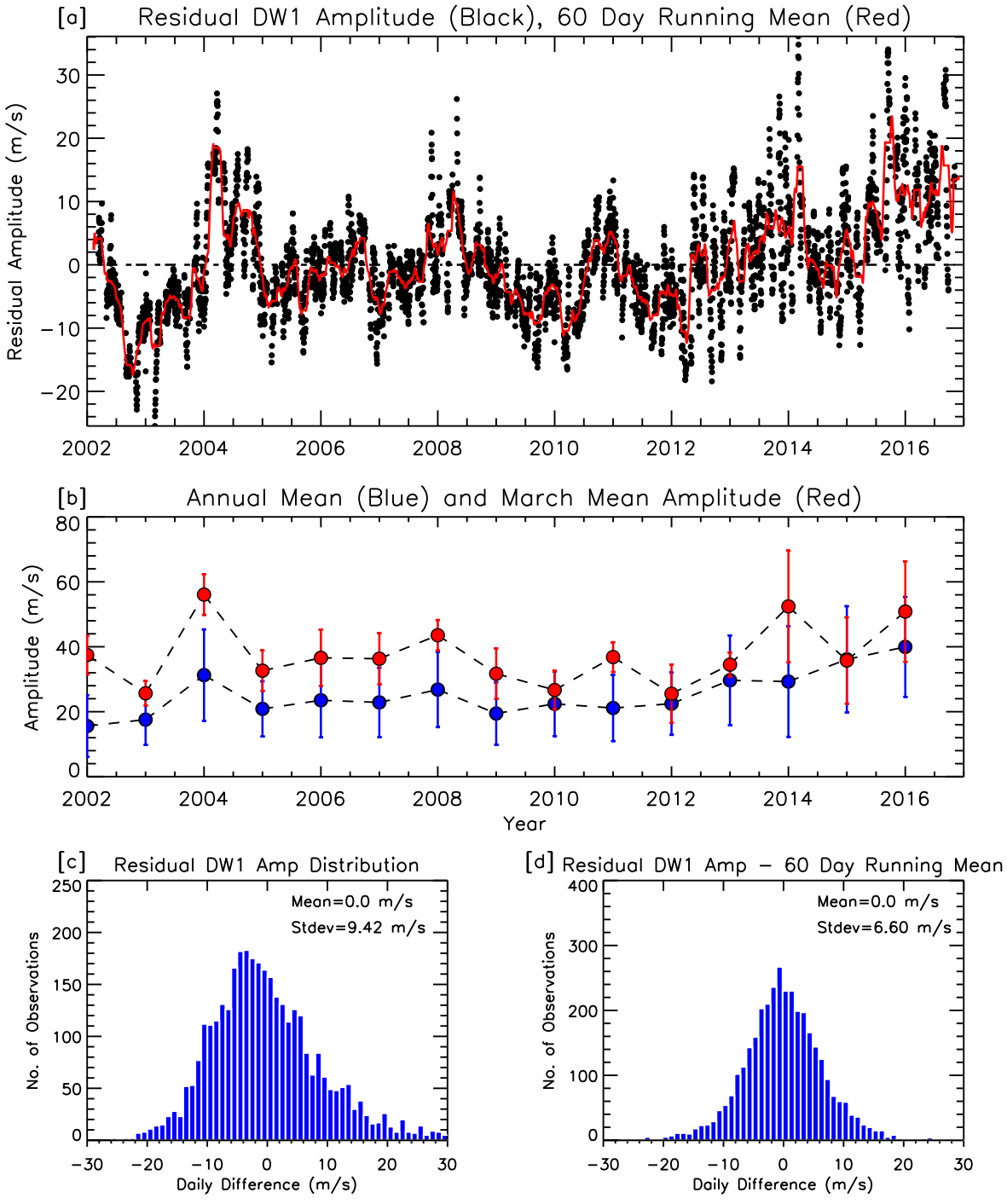

Figure 6. Panel a: TIDI DW1 (1,1) mode residual amplitude and 60 day running mean time series from 2002 to 2016, panel b: TIDI DW1 annual and March mean amplitude. The error bars denote the standard deviation of the estimated tidal amplitudes, panel c: histogram of residual amplitude shown in panel a, and panel d: residual amplitude after removing 60 day running mean (shown in panel a).

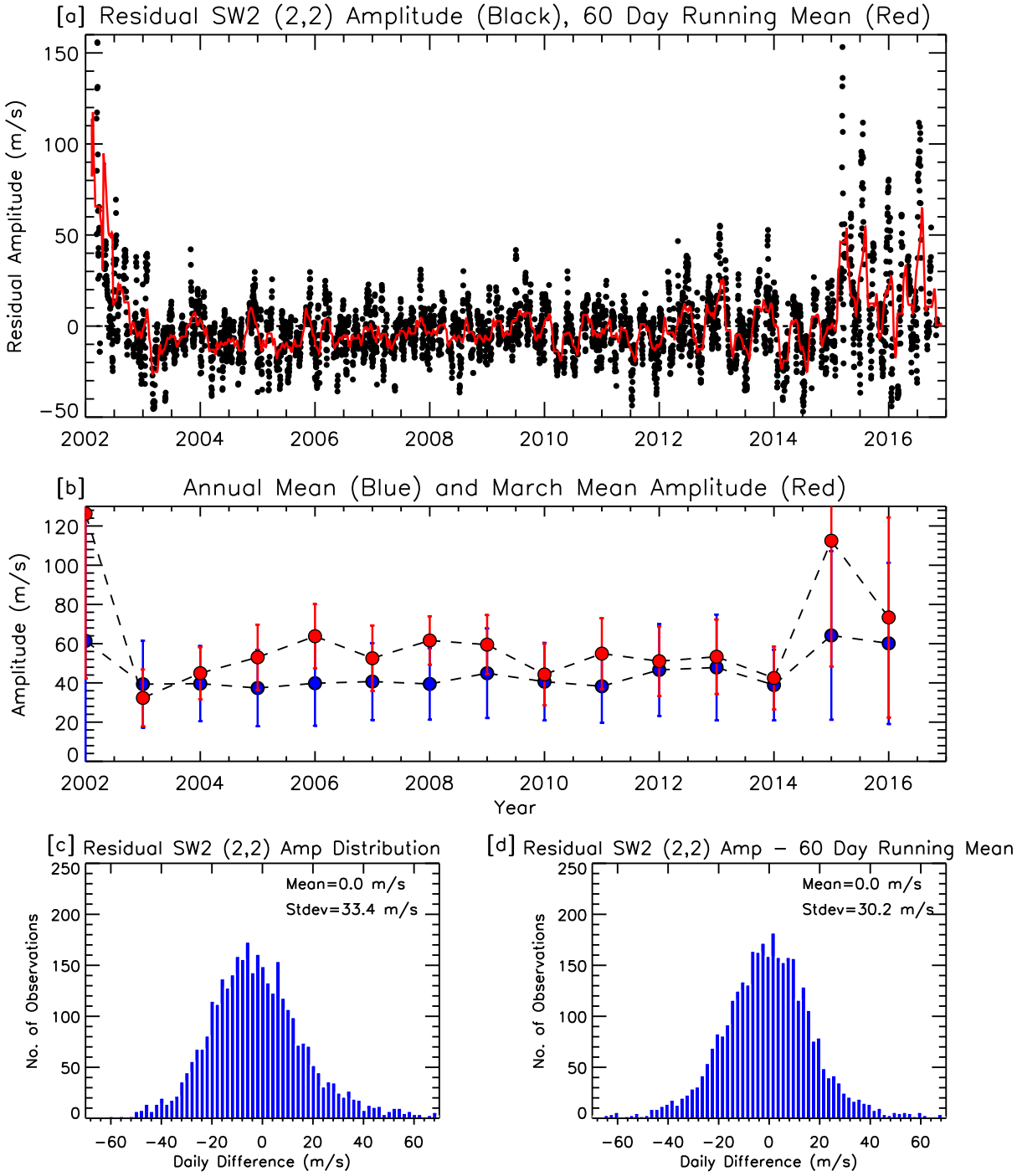

Figure 7. Same as for Figure 6, but here for SW2 (2,2) mode.

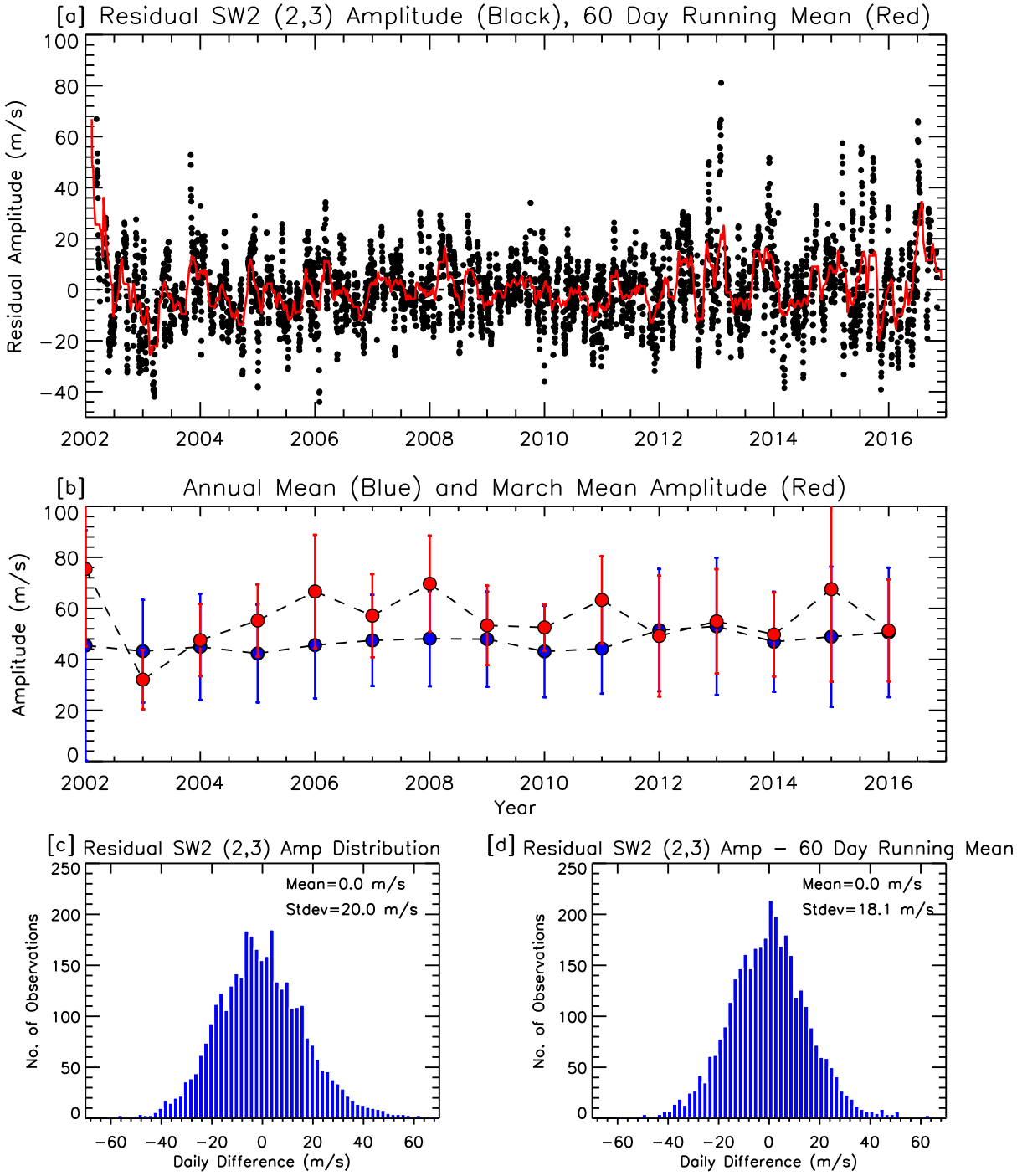

Figure 8. Same as for Figure 6, but here for SW2 (2,3) mode.

Figure 1.

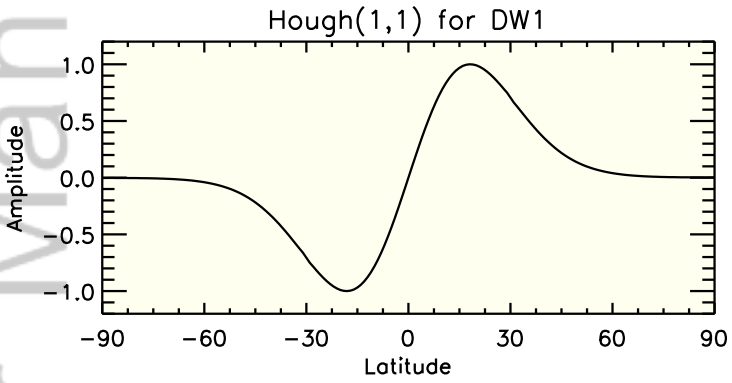

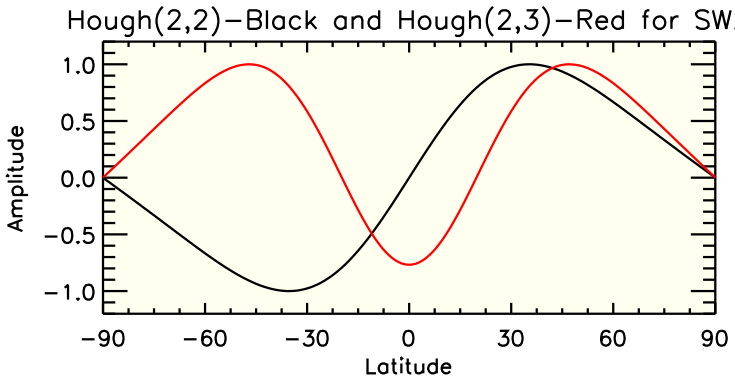

Figure 2.

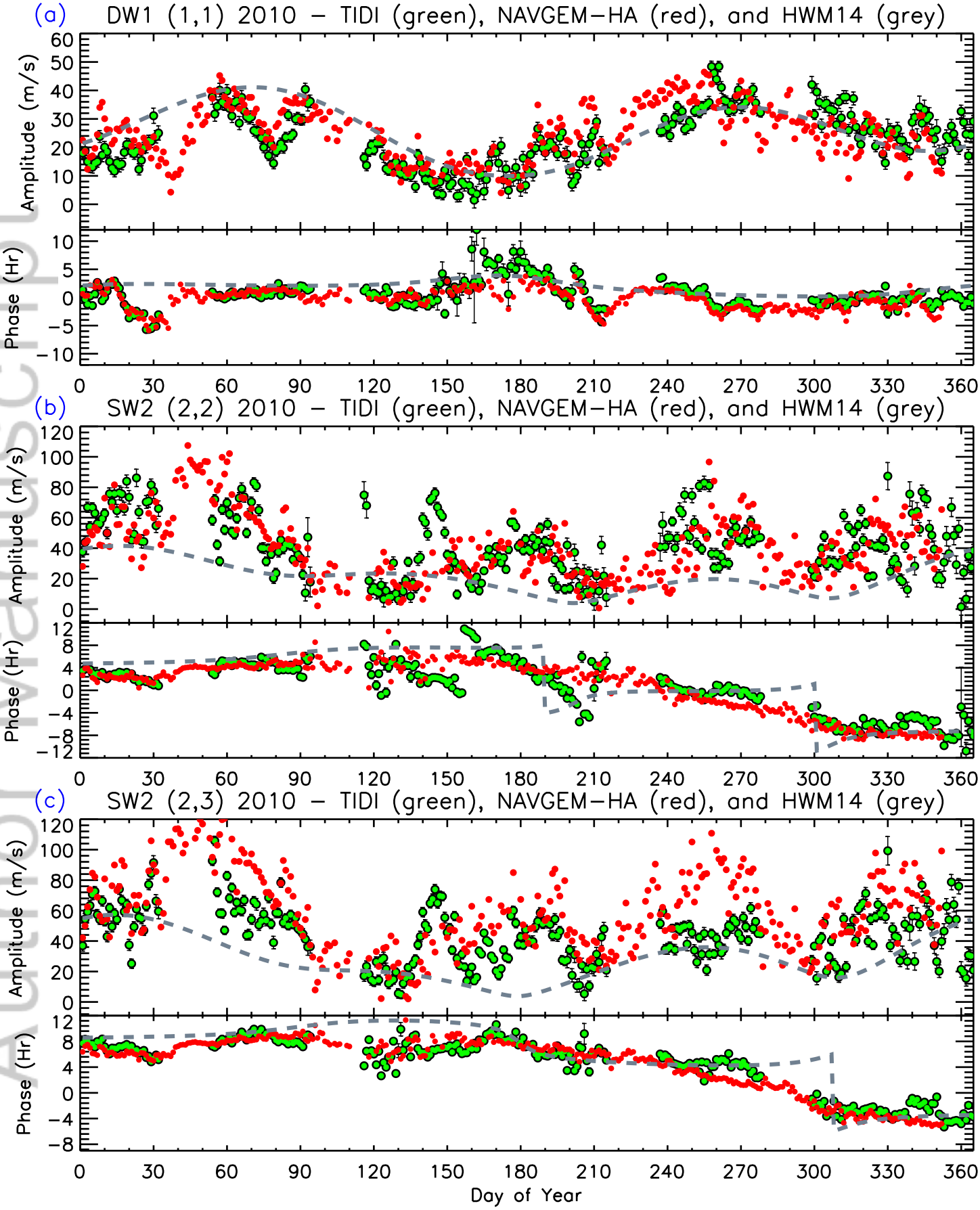

Figure 3.

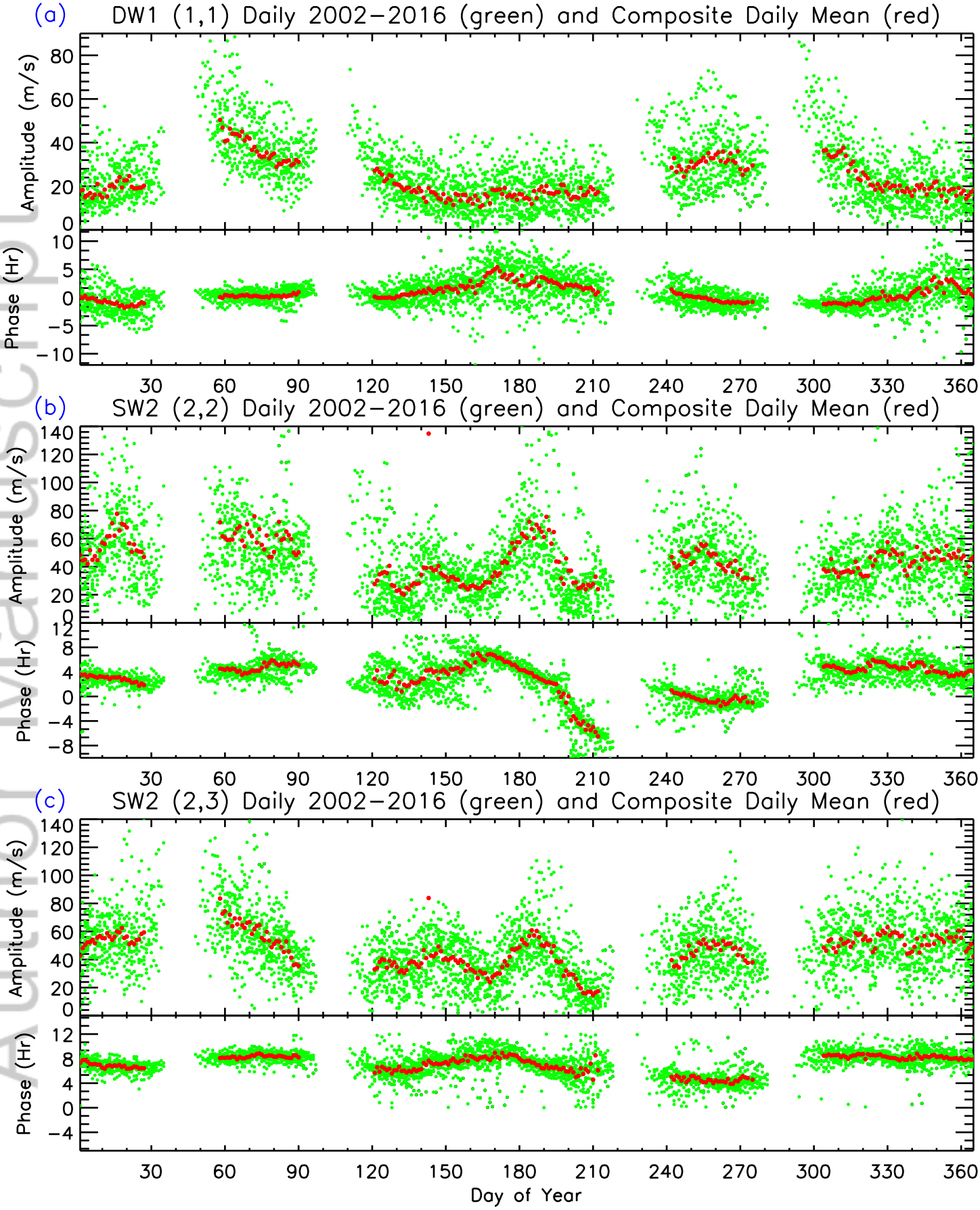

Figure 4.

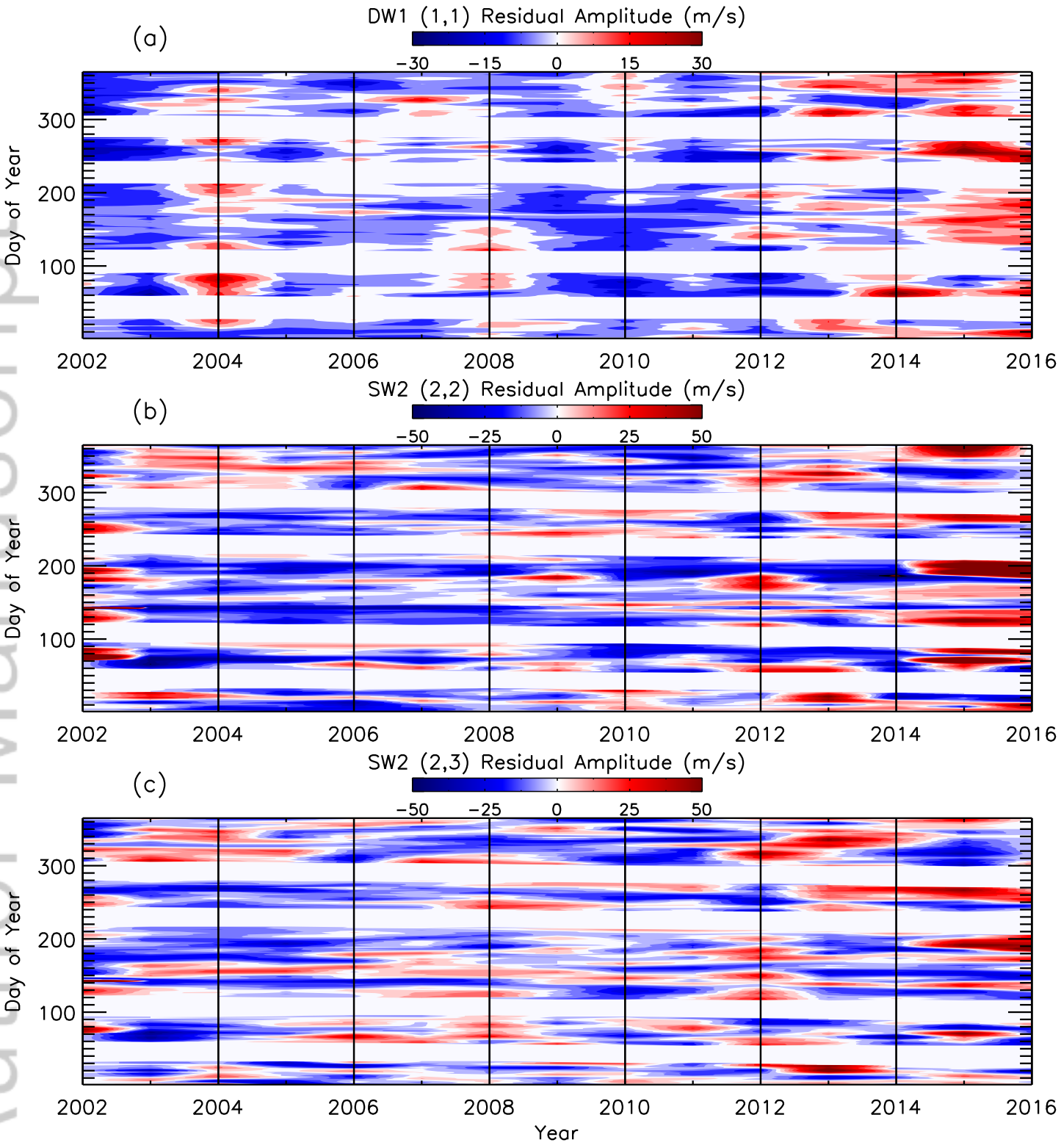

Figure 5.

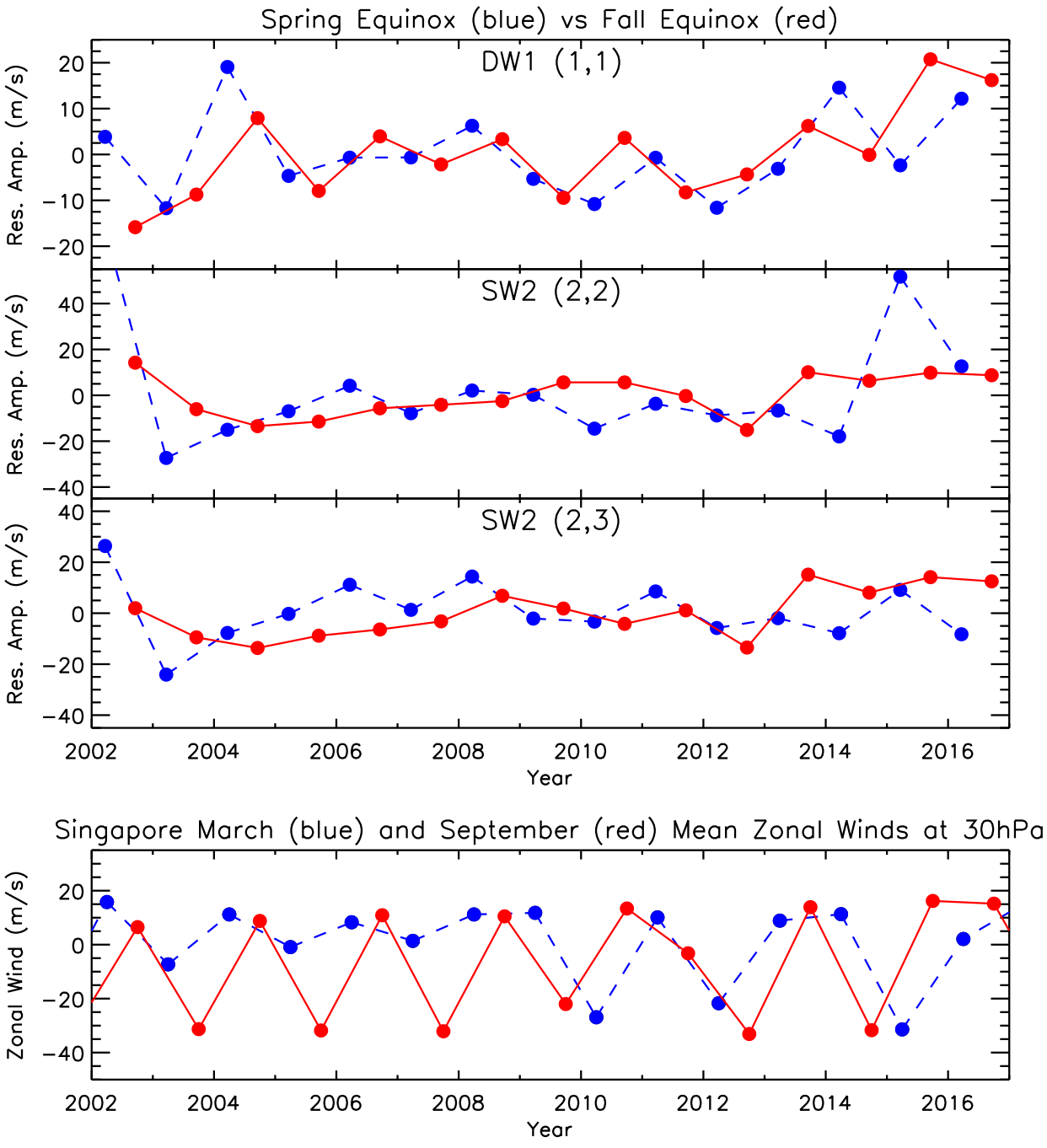

Figure 6.

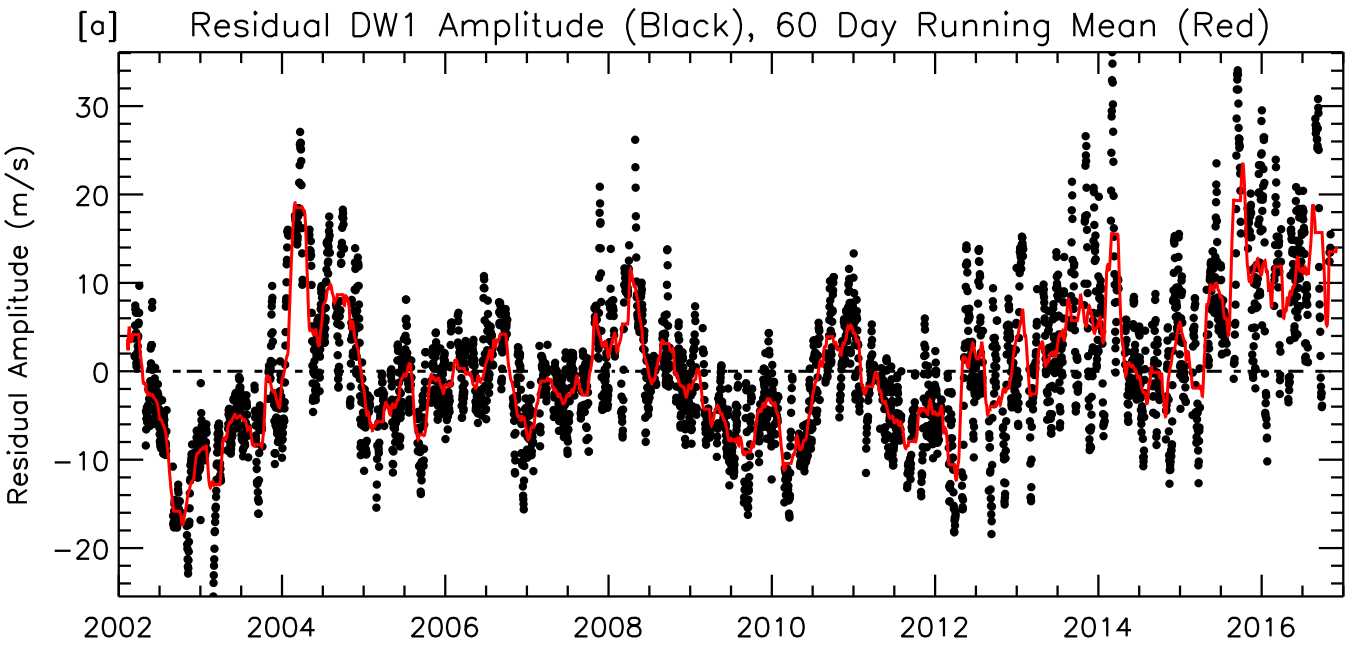

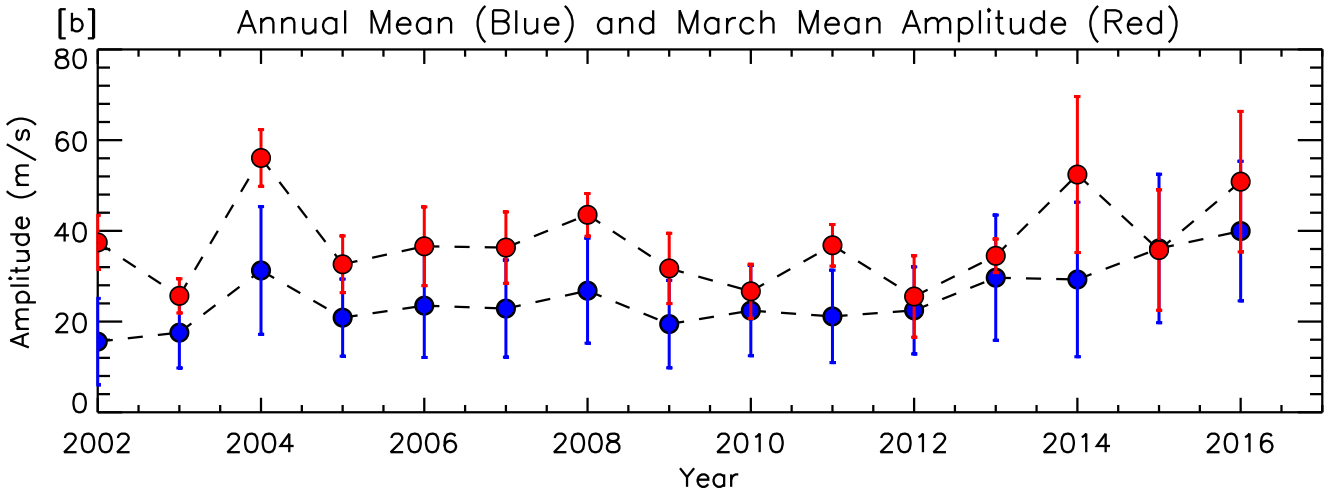

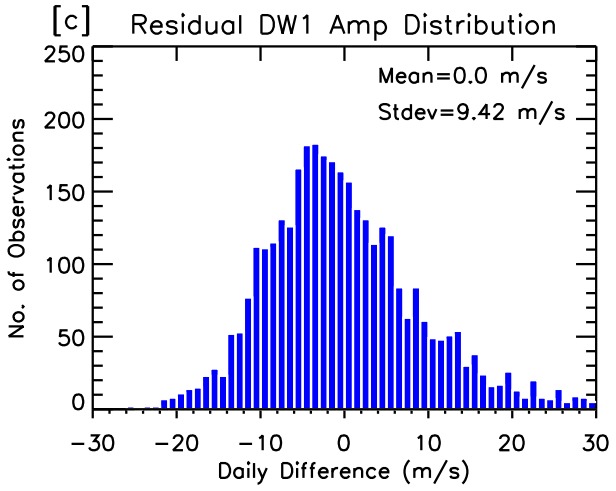

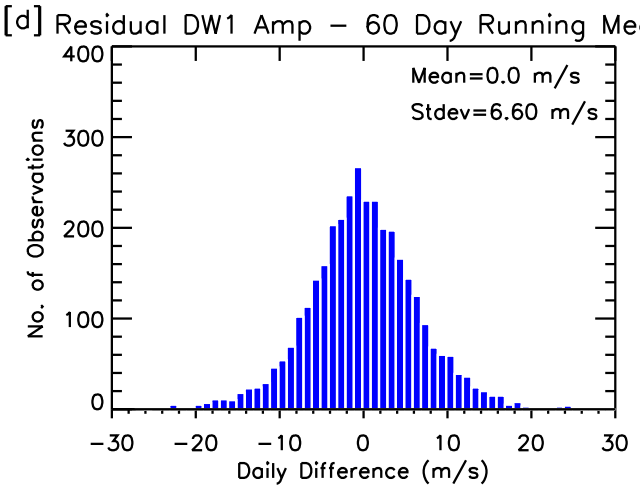

Figure 7.

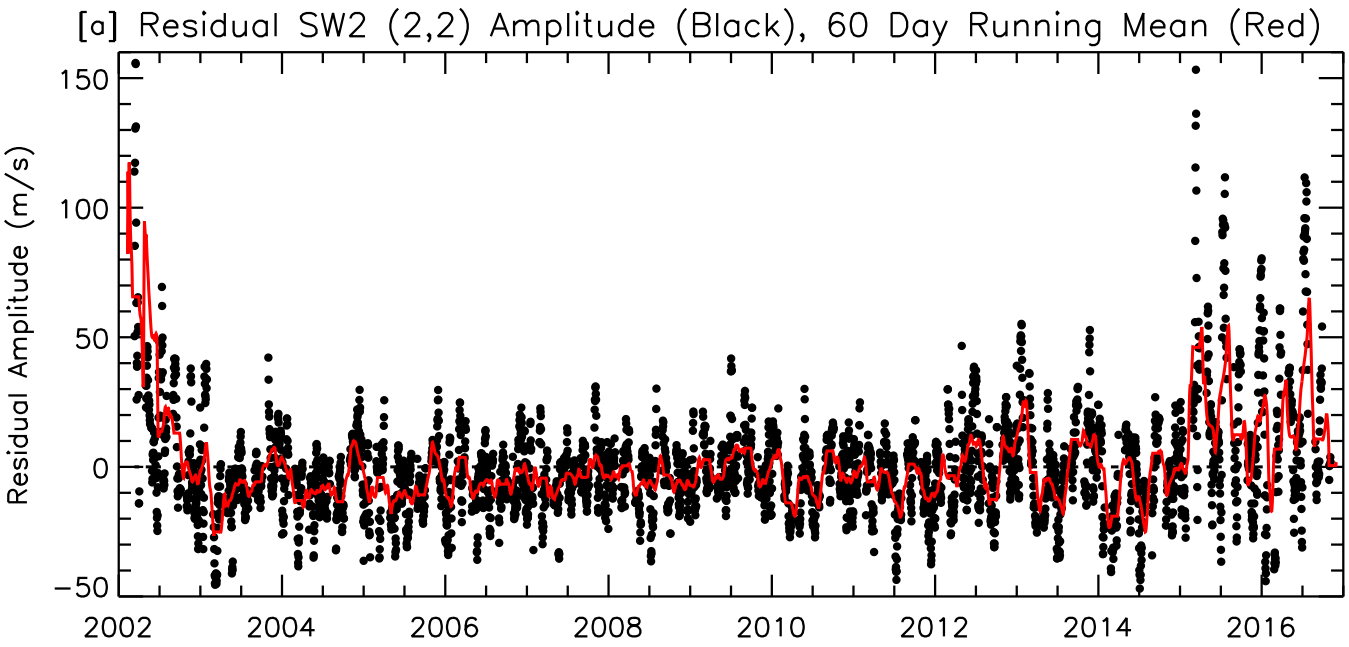

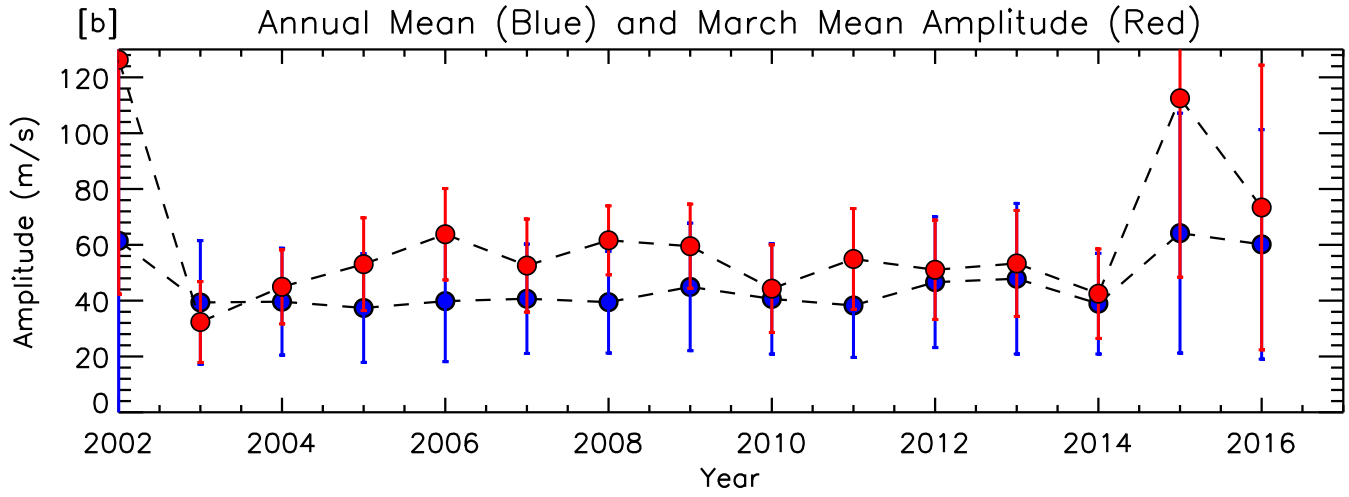

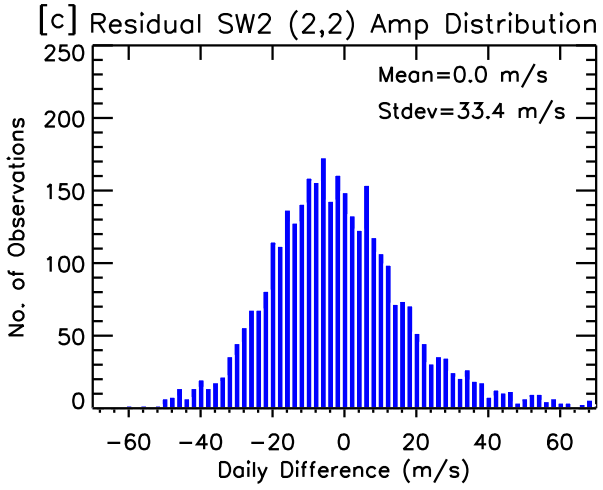

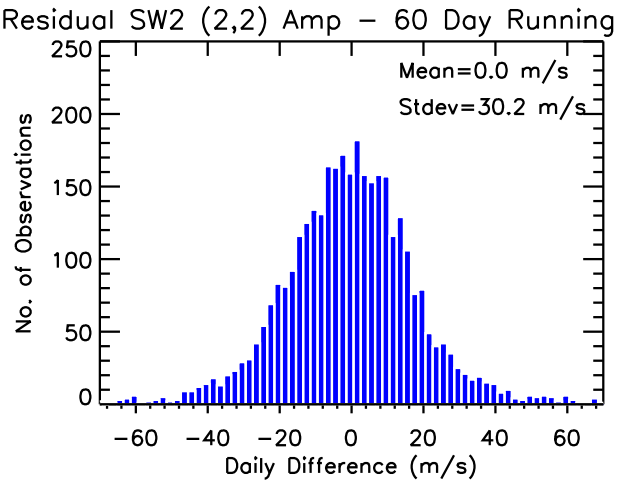

Figure 8.